Materials Advances

Accepted Manuscript

This article can be cited before page numbers have been issued, to do this please use: S. Sheikh, M. Nasiruddin, I. Khan, N. J. Nipa, F. Tul Afroz, M. S. A. Mamun and S. Mansur, *Mater. Adv.*, 2026, DOI: 10.1039/D6MA00326E.

ROYAL SOCIETY OF CHEMISTRY

rsc.li/materials-advances

Recent Advancements in Two-Dimensional Materials for Microfluidic Biosensors: Emerging Trends and Future Perspectives

Samrat Sheikh[1], Md Nasiruddin[2*], Ibrahim Khan[1], Nusrat Jahan Nipa[1], Fatema Tul Afroz[3], Muhammad Shamim Al Mamun[4,5], Syfulla Mansur[6]

Affiliations

[1] Department of Chemistry, Gopalganj Science and Technology University, Gopalganj, Bangladesh

[2] Department of Chemistry, University of Rajshahi, Rajshahi, Bangladesh

[3] Department of Electrical and Electronic Engineering, University of Rajshahi, Rajshahi, Bangladesh

[4]Chemistry Discipline, Khulna University, Khulna, Bangladesh

[5] Department of Chemical and Material Engineering, University of Nevada, Reno, USA

[6] Department of Chemistry, Bangladesh University of Engineering and Technology, Dhaka, Bangladesh

***Corresponding Author:** nasir@ru.ac.bd

Abstract

Microfluidic-based sensors have recently emerged as powerful platforms for rapid, sensitive and miniaturized analytical systems particularly for point-of-care diagnostics and real-time monitoring. The coupling of two-dimensional (2D) layered materials with microfluidic technologies has gained widespread interest due to their distinctive physicochemical properties such as high surface-to-volume ratio, tunable electronic structures, excellent charge transport characteristics, exceptional catalytic activity and abundant active sites for biomolecular interactions. 2D materials beyond graphene such as transition metal dichalcogenides (MoS_2, $MoSe_2$, WS_2), MXene, black phosphorus, metal oxides, graphitic carbon nitride (g-C_3N_4), and layered double hydroxides have demonstrated notable potential for enhancing the sensitivity, selectivity, and response time of microfluidic sensors.

View Article Online
DOI: 10.1039/D6MA00526E

This comprehensive and up-to-date review particularly highlights the scientific advancements in analytical chemistry applications based on beyond graphene 2D materials. Special emphasis is given on electrochemical and optical sensing platforms, their device integration, and biomolecule detection applications. Finally, future perspectives are highlighted to promote the rational design of highly sensitive, portable, and scalable microfluidic sensing platforms for biomedical and environmental monitoring.

Keywords: Microfluidic biosensors; Two-dimensional materials; Lab-on-a-chip; Point-of-care diagnostics; Electrochemical and optical biosensing; MXene.

1. Introduction to Microfluidics and 2D Materials

Microfluidics is a technology that involves the precise processing, manipulation, and control of small volumes of fluids (ranging from 10^{-9} to 10^{-18} L) using a miniaturized system composed of microchannels, chambers, and integrated functional elements.[1,2] This technology has gained widespread attention due to its ability to perform complex laboratory procedure on a single microfluidic chip, known as a lab-on-a-chip (LOC). Microfluidic platforms are widely used in various disciplines, including microelectronics, molecular biology, and biodefense owing to their advantages such as reduced samples and reagents consumption, enhanced accuracy and sensitivity, minimal waste generation, portability, and potential for high throughput analysis. The convergence of innovative design, diverse material selection, and advanced fabrication techniques has revolutionized device performance and functionality, enabling the development of integrated lab-on-chip systems.[3–5] These systems aim to automate and miniaturize conventional laboratory procedures, offering capabilities such as fluid manipulation, mixing, separation, and detection within a compact and portable format.[6]

View Article Online
DOI: 10.1039/D6MA00326E

Since the early 1990s, microfluidics has found its way into biosensing, particularly for point-of-care applications. POC devices utilizing microfluidic systems have emerged as powerful tools for early-stage disease diagnosis, personalized healthcare, and efficient patient monitoring.[7,8] The devices offer real-time results at the site of patient care using minimal biological fluids such as blood, saliva, tears, sweat, and urine. Their compact and integrated design also allows for safe disposal, making them suitable for remote and resource-limited settings, especially during contagious disease outbreaks.[9] In recent years, simpler microfluidic flow systems linked to external sensing modalities have gained preference over complex MEMS-integrated platforms. This shift is driven by the need for more accessible, cost-effective devices, reducing fabrication complexity while maintaining functionality and user-friendliness.[10,11]

One such innovative approach is the development of microfluidic paper-based analytical devices (μPADs), first introduced by Martinez and coworkers.[12] These devices rely on patterned paper substrates that enable fluid transport via capillary action without requiring external pumps or power sources. The use of paper as a substrate offers numerous advantages, including affordability, widespread availability, biocompatibility, and environmental friendliness. Due to their ability to facilitate fluid transport, mixing, and detection within a single compact device, μPADs are particularly suited for resource-limited settings and rapid diagnostics.[13] Various fabrication techniques, such as wax printing, laser cutting, and inkjet printing, have been developed to pattern hydrophobic channels on paper substrates.[14,15] Their inherent porosity, surface chemistry, and compatibility within colorimetric and electrochemical detection methods make them ideal for use in biosensing applications. μPADs have found commercial success in lateral flow assays, such as pregnancy and COVID-19 test strips.[16,17]

Biosensors are analytical devices that combine a biological recognition element with a transducer to detect specific analytes and convert biological interactions into measurable signals.[18,19] These devices are designed for high sensitivity, specificity, reproducibility, and user-friendliness. Depending on the

View Article Online
DOI: 10.1039/D6MA00326E

detection mechanism, biosensors can be classified into electrochemical, optical, piezoelectric, thermal, and field-effect transistor (FET)-based sensors.[20–24] Electrochemical biosensors are widely used due to their high sensitivity, and low detection limits. Optical biosensors offer advantages such as real-time detection, label-free measurements, and high specificity, while FET-based biosensors provide miniaturization potential and fast signal transduction. Initially developed for clinical diagnosis, biosensors have evolved to become more sensitive, stable, and cost-effective owing to advances in material science and device engineering.[25]

In recent years, nanomaterials have been extensively utilized in the development of chemical sensors and biosensors due to their unique physical, chemical, and biological properties. These materials, including nanoparticles, nanotubes, and nanosheets, significantly enhance sensor performance by improving sensitivity, signal amplification, and surface-to-volume ratio.[26,27] Functionalized nanomaterials such as gold (AuNPs) and silver nanoparticles (AgNPs) are commonly employed in microfluidic biosensors due to their tunable optical and electronic properties.[28–30] The integration of these nanomaterials with microfluidic platforms enables precise control of fluid flow, reduced sample volumes, and enhanced detection limits. In optical biosensors, nanomaterials serve as fluorophores, quenchers, or contrast agents, improving signal-to noise ratios and enabling multiplexed detection. In electrochemical biosensors, they enhance electron transfer kinetics, reduce overpotential, and improve signal stability. Furthermore, the use of nanomaterials in microfluidic biosensors facilitates the development of miniaturized, portable, and low-cost diagnosis devices suitable for POC applications.

Among various nanomaterials, two-dimensional (2D) materials have garnered significant attention due to their exceptional physicochemical properties. Since the successful exfoliation of graphene in 2004 by Novoselov and Geim,[31] researchers have explored a wide range of 2D materials beyond graphene, including transition metal dichalcogenides (TMDs), black phosphorus, metal oxides, graphitic carbon nitride (g-C_3N_4), MXenes, and layered double hydroxides. These materials exhibit

View Article Online
DOI: 10.1039/D6MA00326E

atomic or few-atomic-layer thickness, high surface area, superior mechanical strength, and tunable electronic and optical properties, making them highly suitable for applications in energy storage, catalysis, electronics, and biosensing. Due to their tunable bandgap, good electrical conductivity, and strong adsorption capabilities, 2D materials are ideal candidates for developing high-performance biosensors.

2D materials are generally classified into five major groups: (i) graphene and its analogues such as graphitic carbon nitride (g-C_3N_4), hexagonal boron nitride (h-BN); (ii) transition metal dichalcogenides (e.g., MoS_2, WS_2, $MoSe_2$, WSe_2); (iii) transition metal oxides (e.g., ZnO, TiO_2); (iv) black phosphorus; and (v) MXenes.[32,33] Each of these materials possesses unique structural, electronic, and chemical properties that influence their performance in sensing applications. The distinct layer-dependent properties of 2D materials allow for enhanced interaction with biomolecules, resulting in improved sensitivity, selectivity, and stability in biosensor design. The combination of 2D materials with microfluidic platforms further enables the development of integrated, flexible, and multifunctional biosensors for on-site diagnostics and real-time monitoring.

This review aims to provide a comprehensive overview of the recent advancements in 2D materials-based microfluidic biosensors, with a particular focus on electrochemical and optical sensing, as illustrated in Fig. 1. While many reviews exist on 2D materials or microfluidics independently, few explore their convergence for biosensing.[34] The goal of this article is to bridge this gap by examining how the unique properties of 2D materials enhance microfluidic biosensors in terms of sensitivity, selectivity, and scalability. In particular, this review highlights the use of emerging 2D materials beyond graphene, such as MoS_2, WS_2, $MoSe_2$, MXene, phosphorene, and paper-based electrochemical sensors, for the development of wearable and point-of-care biosensing platforms. Furthermore, it addresses the current challenges and limitations in the field and presents future perspectives for the development of integrated, intelligent, and personalized microfluidic biosensing systems.

View Article Online
DOI: 10.1039/D6MA00326E

2. Two-dimensional (2D) Materials

2.1 Structural Properties and Mechanical Behaviour of 2D Materials

Few-atomic-layered 2D materials tightly bound together by van der Waals forces have high flexibility in bending and low rigidity in the plane.[35] They can be aggregated to form vertically aligned heterostructures that have distinct electrical, mechanical and optical properties. These properties are critical when considering 2D materials for biosensing applications because the interlayer shear and buckling effects determine the mechanical performance of the material, which is required for sensor stability and functional performance. For example, buckling causes deformations in the outer plane of the material. This results in a highly flexible material to external load such as strain or fluid flow, which is typically applied in microfluidic devices.

2D materials, such as graphene, hexagonal boron nitride (h-BN), and MoS_2 exhibit unique stress behaviour under stress wherein their in-plane stiffness allows the propagation of ripples rather than crumples as occurs in bulk materials.[36] This unique mechanical behaviour makes 2D materials capable of bearing higher strains than bulk materials and therefore suitable for use in flexible strain

View Article Online
DOI: 10.1039/D6MA00326E

sensitive biosensors. Further, the large surface area of 2D materials facilitates oxidation–reduction reactions and electron migration among others, both key features in biosensors of rapid response.

These unique mechanical and structural features (e. g. exfoliation, deformation behaviour, surface functionalization capability) allow for the development of 2D materials for microfluidic biosensors and other wearable sensing systems. Furthermore, due to their highly sensitive nature to environmental conditions (e. g. water or air) they can provide real -time data in biosensing systems.

2.2 Tuning Properties of 2D Materials for Advanced Biosensors

Transition metal dichalcogenides (TMDs), with the general formula MX_2 (where M = Mo, W, Re and X = S, Se, Te), have emerged as promising 2D nanomaterials for next-generation electronic and biosensing applications.[37] For example, monolayer MoS_2 has a unique sandwich-like structure with a transition metal layer between two chalcogen layers, measuring approximately 0.65 nm in thickness.[38] Unlike its bulk form, monolayer MoS_2 exhibits a direct band gap (~1.8 eV), enabling strong light-matter interactions, fast heterogeneous electron transfer, and excellent optical sensitivity which makes it ideal for high-performance biosensors.

TMDs offer remarkable mechanical, electronic and chemical tuneability. Their band structure can be tuned by strain, doping or alteration of the layer thickness; it can even have ferromagnetic properties under certain conditions. Doping with elements such as nitrogen, oxygen or fluorine enhances electrochemical activity and magnetic moments; nitrogen-doped WS_2 is better at stabilizing and reducing threshold potential and therefore suited for electrocatalysis as well as sensing.

Due to their large surface area and strong Coulombic interactions, TMDs are suitable for holding various functional molecules and can be used in hybrid nanocomposite design.[39] Further, the fact that MoS_2/WS_2 heterostructures can be fabricated on wafer scale by precise layer control provides a new scalable way of fabrication of microfluidic biosensors. To this end, in addition to their high Young's modulus and flexibility, TMDs offer an excellent conformability both for wearable biosensors and

point-of-care devices. Therefore, TMD-based nanostructures based on MoS_2 and WS_2 are promising candidates for developing new generation microfluidic field-effect transistor (FET) biosensors.

MXenes are a class of versatile 2D materials consisting of transition metals, such as Ti, V, Mo, Nb, and carbon or nitrogen, with surface-terminating groups such as -O, -OH, -F, -Cl, and -Br. The general formula for MXenes is $M_{n+1}X_nT_x$, wherein n = 1, 2, 3; and $Ti_3C_2T_X$ is one of the most investigated MXenes owing to its very outstanding properties.[40] Due to their unique laminar architecture, MXenes offer an exceptional platform for immobilizing biological recognition elements, enabling high-performance biosensors. This includes applications in enzyme-based sensors,[41] immunosensors,[42] and small molecule detection,[43] where efficient electron transfer and large surface area are critical. Moreover, MXenes have a large surface area, high hydrophilicity, and flexibility. The active biochemical catalysis and semiconducting nature as well as the ability to produce reactive oxygen species are further reasoned for their applications in sensor fabrication. Other 2D materials that have been less often integrated with LOC devices exhibiting unique structural features may enhance the functionalities of microfluidic biosensors.

Importantly, the physicochemical properties of MXenes are strongly governed by their surface terminations and transition metal core. The presence of –O, –OH, and –F groups not only enhance hydrophilicity but also significantly modifies the surface electronic states, thereby tuning the work function and interfacial charge transfer behavior.[44] This surface chemistry is also responsible for their high-water affinity and facile functionalization, which is advantageous for biosensor fabrication in aqueous environments.

Compared to graphene, MXenes exhibit a fundamentally different electronic structure due to the presence of transition metal d-electrons, which contribute to metallic conductivity and higher electrochemical activity. In contrast, graphene requires chemical modification (e.g., graphene oxide or reduced graphene oxide) to improve dispersion, which often compromises its conductivity.[45]

View Article Online
DOI: 10.1039/D6MA00326E

MXenes, however, can simultaneously maintain high conductivity and stable dispersion, making them more suitable for solution-processed biosensing platforms.

Black phosphorus (BP) nanosheets exhibit a zigzag sheet structure wherein each of the phosphorus atoms is covalently bound to three adjacent phosphorus atoms.[46] The impressive electronic and optoelectronic properties which are readily available on such nanosheets are described in terms of their potential biosensing use. BP exhibits strong in-plane anisotropy arising from its puckered crystal structure, leading to distinctly different physical properties along the armchair and zigzag directions. This anisotropic nature significantly influences charge transport, optical response, and carrier mobility, making BP highly attractive for direction-dependent sensing applications.

Unlike graphene, which is characterized by a zero-band gap, BP possesses a thickness-dependent direct band gap ranging from approximately 0.3 to 2.0 eV.[47] This tunable band structure enables BP to bridge the electronic properties between graphene and transition metal dichalcogenides, thereby offering a unique advantage for optoelectronic and electrochemical biosensors. In addition, BP shows strong molecular adsorption capability and relatively high carrier mobility, which enhance its sensitivity toward analyte detection.

However, a major limitation of BP is its inherent environmental instability, as it undergoes rapid oxidation in the presence of oxygen and moisture, which restricts its long-term practical applications unless appropriate passivation strategies are employed.[48]

Like BP nanosheets, the semiconducting 2D material g-C_3N_4 exhibits a graphene-like design induced by the sp^2-hybridized C-N bonds.[49] It is the first semiconducting 2D material to exhibit heptazine-based architecture. Its electrical and optical properties make it a promising target for sensing applications. 2D Metal-Organic Frameworks (MOFs) have large crystals composed by polymerization of metal ions and organic ligands.[50] Such structures have potential use in biosensors. Although only a few experimental studies have been performed to integrate these 2D materials with

View Article Online
DOI: 10.1039/D6MA00326E

LOC devices, these 2D materials present promising traits which will provide an avenue for future research toward the advancement of microfluidic biosensors.

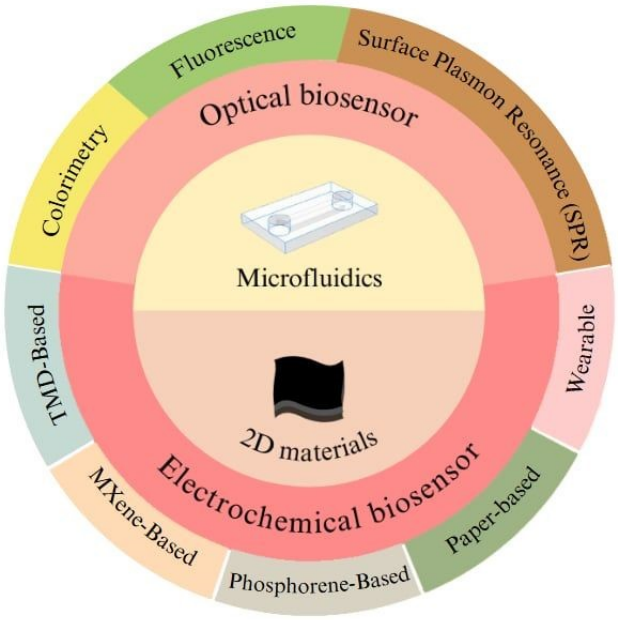

Fig. 1 Schematic representation of the integration of two-dimensional (2D) materials with microfluidic lab-on-a-chip (LOC) platforms for advanced biosensing applications.

2.3 Comparative physical properties and biosensing advantages of selected 2D materials

The intrinsic physical properties summarized in Table 1 highlight the complementary advantages of different 2D materials for biosensing applications. In particular, MXenes provide superior electrical conductivity and rich surface chemistry, enabling efficient charge transfer and effective biomolecule immobilization in electrochemical sensing platforms. Black phosphorus (BP) offers thickness-dependent bandgap tunability and pronounced in-plane anisotropy, which enhance its sensitivity in field-effect transistor (FET)-based and optoelectronic biosensors. Transition metal dichalcogenides (TMDs), such as MoS_2 and WS_2, combine a direct bandgap with excellent semiconducting behavior,

View Article Online
DOI: 10.1039/D6MA00326E

making them suitable for optical and electronic sensing devices. In contrast, graphene serves as a benchmark material owing to its exceptional conductivity and mechanical strength, despite its zero-bandgap limitation.

Fig. 2. presents a comparative schematic of the atomic structures of key 2D materials, including graphene, MoS_2, MXenes, and black phosphorus, emphasizing their structural diversity and functional relevance in biosensing platforms.

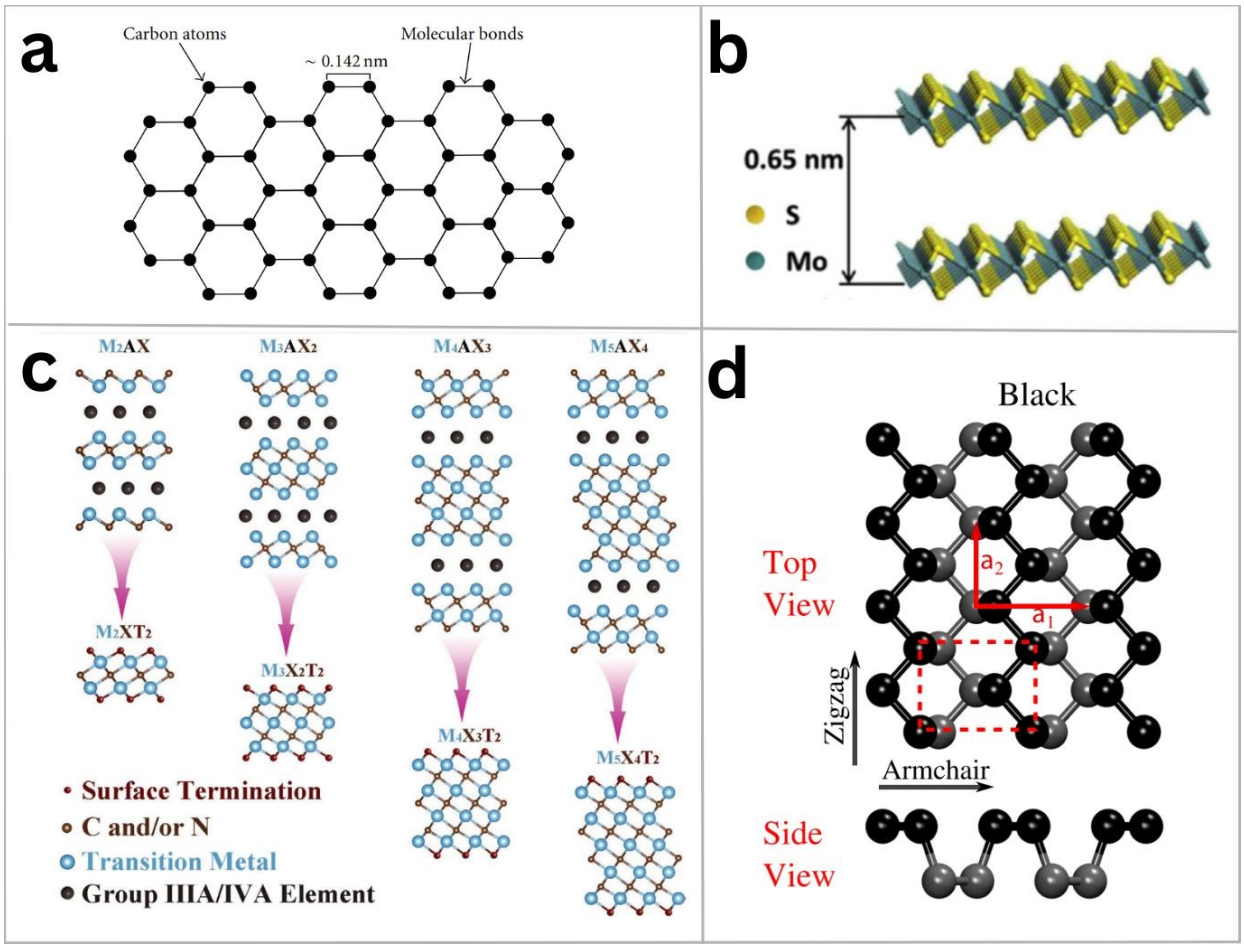

Fig. 2 Schematic illustration of the atomic structures of selected two-dimensional materials: (a) graphene, where carbon atoms are arranged in an sp^2-hybridized honeycomb lattice and bonded to neighboring atoms;[51] (b) molybdenum disulfide (MoS_2), a representative transition metal dichalcogenide (TMD) with a layered structure and an interlayer spacing of ~0.65 nm;[51] (c) general atomic structures of MXenes with different stoichiometries (M_2AX, M_3AX_2, M_4AX_3, and M_5AX_4);[52]

View Article Online
DOI: 10.1039/D6MA00326E

(d) puckered honeycomb structure of black phosphorus (BP), exhibiting strong in-plane anisotropy along the armchair and zigzag directions.[53] Adapted from Refs. 51–53 with permission.

View Article Online
DOI: 10.1039/D6MA00326E

Table 1: Comparative overview of structural, electronic, surface, and mechanical properties of selected two-dimensional materials highlighting their key advantages for biosensing applications.

Material	Structure / Thickness	Bandgap	Conductivity	Surface Chemistry / Functionalization	Mechanical Properties	Key Biosensing Advantage	Reference
MXenes ($Ti_3C_2T_X$)	Layered laminar structure; thickness 1–5 nm	Metallic / tunable	Very high (~10^4 S/cm)	–O, –OH, –F, –Cl, –Br surface terminations	High flexibility, good strain tolerance	Excellent electrochemical sensing, fast electron transfer, enzyme immobilization, hybrid nanocomposites	54
Black Phosphorus (BP)	Zigzag sheet; few-layer 0.5–2 nm	0.3–2 eV (thickness-dependent)	Moderate	Reactive edges; oxidation-prone	Moderate flexibility, anisotropic behavior	FET-based and optoelectronic biosensors; anisotropic charge transport, high optical sensitivity	55
TMDs (MoS_2, WS_2, WSe_2)	Sandwich-like monolayer (0.65 nm)	1.8 eV (monolayer, direct)	Moderate	Limited functional groups; can be doped (N, O, F)	High Young's modulus; flexible	FET-based biosensors, hybrid nanocomposites, strain-tunable properties, optical and electrochemical sensing	56
Graphene	Single-layer hexagonal carbon lattice	0 eV	Very high	Inert; can be functionalized (–OH, –COOH)	Very high in-plane stiffness; strong, flexible	Conductivity benchmark, structural support, electrochemical sensing platform	57

View Article Online
DOI: 10.1039/D6MA00326E

g-C_3N_4	Heptazine-based layered structure	2.7 eV	Moderate	N-rich surface for functionalization	Moderate stiffness; good thermal stability	Photocatalytic and optical biosensing; hybrid sensor design	58
2D MOFs	Coordination network of metal ions + organic ligands	Tunable	Moderate	Highly tunable organic linkers	Moderate mechanical stability	Enzyme immobilization, molecular recognition, optical and electrochemical sensing	59

Overall, the selection of 2D materials for biosensing should be guided by their intrinsic electronic, surface, and mechanical properties rather than a single performance metric. This comparative understanding provides a rational framework for designing next-generation microfluidic and wearable biosensors with optimized performance.

3. Harnessing 2D Layered Materials for Advanced On-Chip Electrochemical Sensing

Unlike graphene, which has a zero-band gap, other 2D materials offer a distinct advantage in electrochemical systems due to their intrinsic non-zero band gap.[60,61] This key property enables precise tuning of electronic and electrochemical behaviour, allowing for enhanced charge transfer and improved sensor performance. Such materials not only act as efficient sensing elements but also provide a stable platform for immobilizing bio-recognition molecules, making them highly suitable for advanced electrochemical biosensing applications.[62] This is typically performed by depositing the nanomaterials onto the electrode's active surface through drop-casting, followed by performing electrochemical measurements. For Field-effect transistor (FET)-based sensors, nanomaterials are generally exfoliated layer by layer using the Scotch tape or chemical vapor deposition (CVD)

View Article Online
DOI: 10.1039/D5MA00326E

method. For MXene, single or few-layer nanosheets are obtained by using an intercalating agent (e.g., TBAOH, DMSO, or LiCl) which weaken interlayer interactions, followed by mild sonication or mechanical shaking to further separate the layers into individual nanosheets. Single or few-layered nanomaterials are positioned across the interface separating the source and drain electrodes of the device.

Then an electrochemical test is performed for the detection of a target analyte, introduced either by drop-casting or using a microfluidic platform powered by a syringe pump.[63] The attractive traits of TMDs include high conductivity, versatile functionalization, and ultrathin features that carve them as attractive materials for the construction of biosensor devices due to the capability of enabling rapid electron transfer and increased sensitivity going forth for detection of analytes with low concentrations. Upon functionalization with specific biomolecules or nanoparticles, selectivity, and recognition capabilities can be further enhanced, allowing biosensing platforms with a greater degree of accuracy and reliability. Moreover, the flexibility and scalability of TMDs allow the integration of flexible and wearable devices for real-time diagnosis at the point of care.[64]

3.1 Transition Metal Dichalcogenide (TMD)-Based Microfluidic Biosensors

3.1.1 MoS_2-Based Microfluidic Biosensors

Hussain et al. present a highly sensitive and reusable MoS_2-based field-effect transistor (FET) biosensor for detecting bisphenol A (BPA), an environmental contaminant linked to serious health issues (Fig. 3a).[65] The device was fabricated using mechanically exfoliated multilayered MoS_2 on a Si/SiO_2 substrate, with high-density AuNPs deposited via e-beam evaporation to improve electrical contact. Annealing at 200°C for 2 hours optimized metal-MoS_2 interface. Functionalization involved immobilizing ss-DNA on MoS_2 for specific BPA interaction. A PDMS microfluidic channel (80 µm × 20 µm) enabled complementary DNA injection, forming ds-DNA probes that enhanced sensitivity via p-doping. A gradual current drop was observed across the MoS_2-FET, correlating with BPA

View Article Online
DOI: 10.1039/D6MA00326E

concentrations from 1 pg/mL to 1 µg/mL. The microfluidic system provided controlled fluid flow and real-time, label-free detection. The ssDNA/dsDNA-functionalized MoS_2 FET achieved a record-low detection limit of 1 pg/mL.

Liang et al. developed a MoS_2 transistor biosensor for detecting Tumor Necrosis Factor-alpha (TNF-α), a key cancer biomarker (Fig. 3b).[66] A few-layer MoS_2 flake was printed on a Si/SiO_2 substrate to create a transistor biosensor. Controlling the MoS_2 flake thickness (15-20 nm) enhanced field-effect mobility. The device featured metallic source/drain contacts and a back-gated MoS_2 channel, with a 30 nm HfO_2 layer deposited for biofunctionalization. A PDMS microfluidic channel was integrated for stable fluid flow and real-time measurement of antibody-TNF-α binding kinetics. The sensor tested TNF-α concentrations from 60 fM to 3 pM, achieving a 60 fM detection limit. Selectivity was confirmed by minimal nonspecific Interleukin-6 (IL-6) binding. The sensor's response was independent of HfO_2 thickness, with consistent results at 30 nm and 60 nm. Performance dependent heavily on transistor properties, highlighting the need for improved fabrication consistency. This study demonstrated the promise of MoS_2 transistors for sensitive and selective biomarker detection.

In addition to TNF-α detection, the same group further advanced their MoS_2-based FET biosensor technology by developing a continuous, time-dependent detection technique (Fig. 3c).[67] This method enabled rapid, low-noise, and highly selective biomolecular detection in complex samples, achieving a 1 fM detection limit with analysis completed within 23 minutes for streptavidin–biotin and IL-1β interactions.

View Article Online
DOI: 10.1039/D6MA00326E

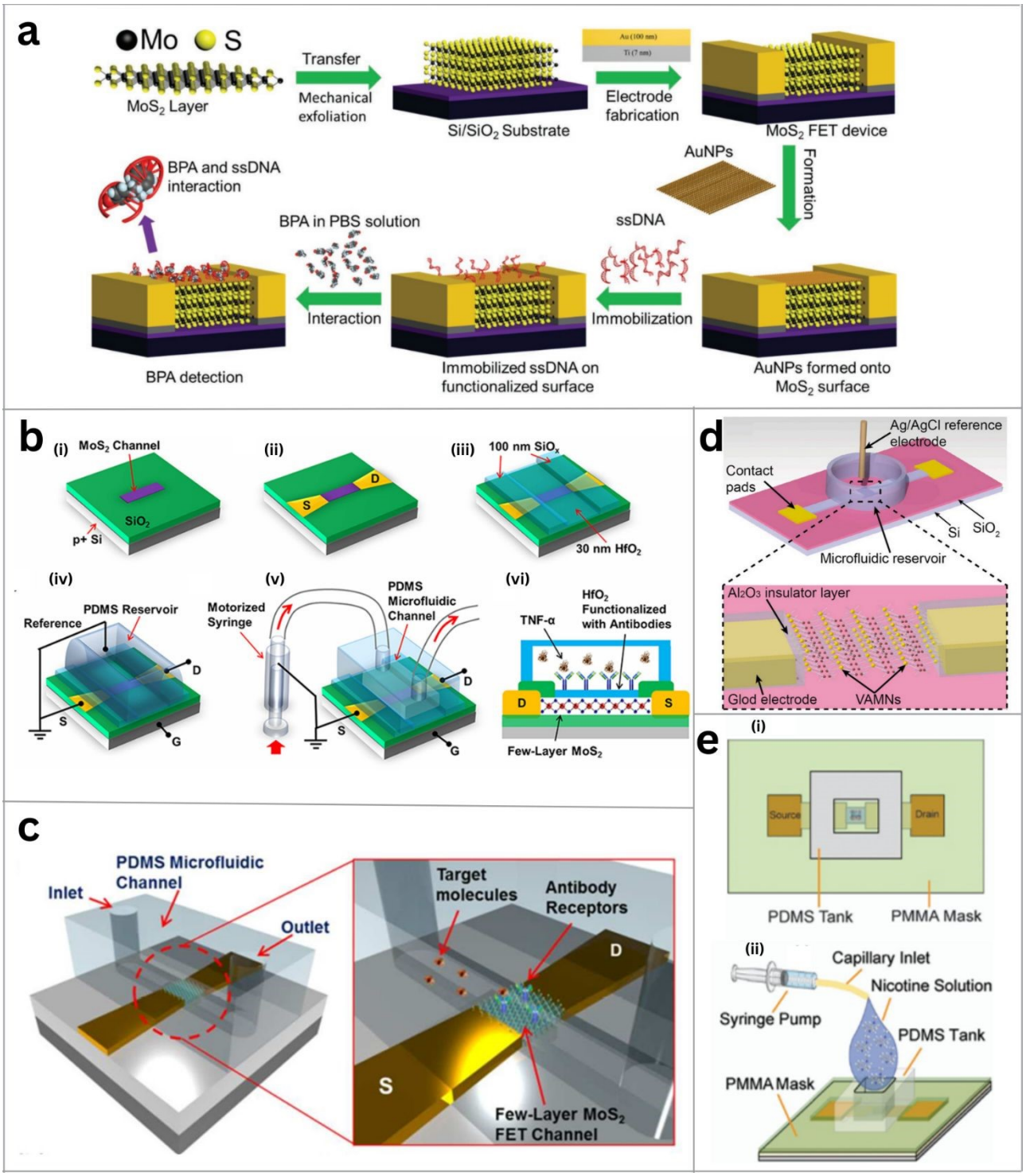

Fig. 3 MoS_2-based FET biosensors in microfluidic applications: (a) Fabrication schematic of a PDMS microfluidic MoS_2-FET device and BPA detection via ssDNA immobilization on the MoS_2-functionalized surface.[65] (b) Illustration of a PDMS microfluidic FET biosensor with a SiO_2 substrate and MoS_2 channel including source, drain, and gate electrodes for TNF-α detection.[66] (c) Representation of a biosensing device for detecting target molecules (IL-1β) flowing through a

View Article Online
DOI: 10.1039/D6MA00326E

PDMS microfluidic channel using a few-layer MoS_2 FET as the sensing channel.[67] (d) Illustration of a MoS_2-FET-based biosensor featuring a PDMS circular reservoir with a solution capacity of 50 mL.[68] (e) Schematic of a microfluidic MoS_2-FET device with a PDMS reservoir for nicotine detection.[69] Adapted from Refs. 65–69 with permission.

The biosensor employs a PDMS microfluidic channel system, delivering reagent for real-time measurement via incubation-flushing-drying-measurement (IFDM) cycles, minimizing electrochemical degradation and nonspecific adsorption. Higher streptavidin concentrations led to greater binding and biotin receptor occupancy. For IL-1β detection, MoS_2 was directly modified for antibody attachment, omitting the hafnium oxide layer.

The sensor was tested at various analyte concentrations, and dissociation kinetics were analyzed with deionized water. Stable performance was maintained for 50 minutes before MoS_2 layer degradation. Despite this, the FET biosensor demonstrated high sensitivity and strong potential for streamlined, reproducible biomolecule detection.

Unlike most microfluidic FET-biosensors requiring precise liquid flow control, constructing a micro-engineered reservoir over the FET device offers an alternative, mitigating challenges tied to traditional inlet-outlet flow dynamics. In this regard, Song et al. introduced a novel FET biosensing channel using vertically aligned MoS_2 monolayers (VAMNs) for detecting prostate-specific antigen (PSA) in human serum (Fig. 3d).[68] This is the first reported use of VAMSs in biosensing. VAMSs were synthesized from a pre-patterned 15 nm Mo film via rapid sulfurization using CVD. The FET used a PDMS microfluidic reservoir (2 mm × 15 mm), with 50 µL capacity. A 30 µL serum sample enabled rapid PSA detection in under 20 minutes, achieving an LOD of 800 fg mL^{-1}, representing a tenfold better than ELISA kits.

Mamun et al. designed a PMMA mask to protect the source and drain electrodes of a MoS_2-based FET from fluid-induced channel damage (Fig. 3e).[69] A PDMS-based microfluidic reservoir was also incorporated to control liquid flow and better target the MoS_2 channel. MoS_2 flakes were transferred onto a Si/SiO_2 substrate using the scotch tape method, with Ti/Au electrodes deposited and PMMA A6 layers formed via spin coating. A microfluidic tank was fabricated on top, sealed with conductive

View Article Online
DOI: 10.1039/D6MA00326E

glue, and heated at 150°C for an hour. A syringe pump injected nicotine solution at 1 µL/hour to ensure focused interaction with the MoS_2 channel. Although the sensor detected 0.6 mM nicotine solution effectively, channel breakage was observed attributed to mechanical issues or weak van der Waals interactions. This method shows promise for in-vivo molecular detection.

A microfluidic MoS_2-FET-based reversible biosensor was also reported for detecting uric acid (UA) detection, a gout marker (Fig. 4a).[70] To improve device stability, they designed a robust FET that remained intact and functional in a liquid environment. UA solution was prepared using isopropyl alcohol (IPA) as the solvent. The FET channel was constructed with MoS_2 nanoflakes, while a microfluidic channel made of PDMS (50 × 40 µm) ensured precise flow condition. To prevent channel damage, the drain and source electrodes were shielded from direct contact with the solution, without affecting electrical behavior.

Changes in FET properties due to UA adsorption were monitored by shifts in the drain current (I_d) vs. gate voltage (V_g) curve, where a leftward shift indicated UA's donor behavior. Reproducibility of the electrical response was demonstrated through multiple cycles, confirming full UA removal after 30 minutes of IPA washing. A higher flow rate of 100 µL/hour enabled a low detection limit of 60 nM without compromising device's performance. The device remained functional for several days in the microfluidic environment under suitable flow conditions.

Liu and coworkers developed a versatile microfluidic MoS_2 FET-based DNA biosensor for noninvasive prenatal detection of Down syndrome (trisomy 21) (Fig. 4b).[71] Monolayered MoS_2, synthesized via CVD, was integrated into a PDMS microfluidic system with inlet/outlet tubes to

control flow rate. The sensor area was exposed for direct testing at the sampling station. Optimally

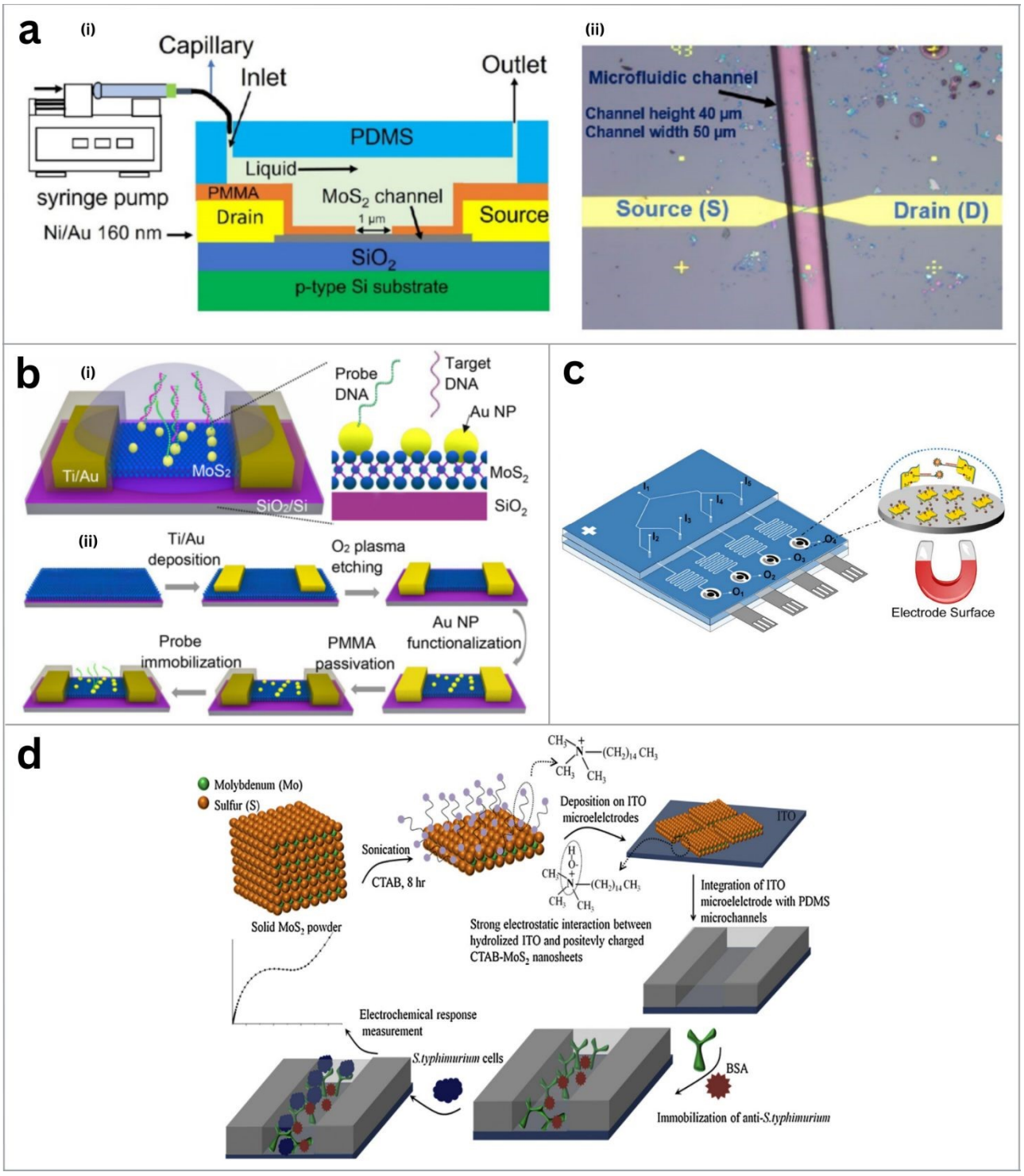

Fig. 4 MoS_2-based biosensors integrated with microfluidic platforms for diverse bioanalytical applications: (a) Schematic illustration of a MoS_2-FET-based biosensor with a PDMS microfluidic channel for uric acid detection.[70] (b) Fabrication of an AuNP-functionalized MoS_2-based FET device via DNA probe immobilization between the source and drain electrodes for effective electrochemical (EC) analysis in Down syndrome screening.[71] (c) Schematic representation of a MoS_2-based biosensor for miRNA detection with a PDMS microfluidic channel comprising five inlets (I1–I5),

View Article Online
DOI: 10.1039/D6MA00326E

four outlets (O1–O4), and integrated sensing electrodes.[72] (d) Schematic design of a MoS_2-based microfluidic biosensor for detecting *S. typhimurium*.[73] Adapted from Refs. 70–73 with permission.

sized AuNPs were deposited on MoS_2 as linkers for DNA probes via Au-S bonds. Target DNA from chromosomes 21 or 13 caused a concentration-dependent current drop due to MoS_2 p-doping. The platform reached a detection limit below 100 aM with up to 240% signal enhancement. Its adaptability via probe modification makes it a cost-effective, programmable alternative to traditional whole genome sequencing (WGS)-based diagnosis.

Besides serving a key material for FETs, MoS_2 nanostructures are widely used to modify electrodes for electrochemical sensing, including voltammetry and impedance techniques. Integrated into microfluidic flow cells, these modified electrodes provide a simpler, cost-effective alternative to FETs, with the added advantage of easy replacement. Electrochemical methods further expand MoS_2's biosensing potential by leveraging its high conductivity and surface reactivity.

Chand et al. introduced a microfluidic electrochemical biosensor based on MoS_2–$CuFe_2O_4$ nanoparticles for the sensitive detection of paratuberculosis (pTb) miRNA205 (Fig. 4c).[72] The system integrates functionalized MoS_2 monolayers enhanced with $CuFe_2O_4$ to improve conductivity and catalytic activity. MoS_2 nanosheets were treated with 2 μM molecular probes and 0.2 mM ferrocene, then immobilized on a screen-printed carbon electrode (SPCE) via electropolymerization. The microfluidic chip (200 μm wide × 100 μm high) enabled continuous analyte flow, improving reproducibility. Electrochemical detection using CV and SWV with $[Fe(CN)_6]^{3-/4-}$ showed a cathodic peak at 0.32 V due to ferrocene oxidation. Optimization of probe, magnetic bead (50 μg/mL strp-MMBs), and flow rate (50 μL/hour) achieved a linear range of 1 pM to 1.5 nM with an LOD of 0.48 pM. Tests with spike serum showed 2-5% error, confirming clinical relevance. Compared to fluorescence or immunosensing, this platform offers superior selectivity, especially in the early pTb detection.

View Article Online
DOI: 10.1039/D6MA00326E

Another example is the surfactant-assisted exfoliation of 2D MoS_2. Singh et al. developed cetyltrimethyl ammonium bromide (CTAB)-functionalized MoS_2 nanosheets (CTAB-MoS_2-NS) for detecting *Salmonella typhimurium* (Fig. 4d).[73] CTAB, added during sonication, stabilizes exfoliated MoS_2 by introducing positive charges that prevent restacking. These positively charged nanosheets interact electrostatically with negatively charged OH groups on hydrolysed indium tin oxide (ITO), enabling smooth electrophoretic deposition onto ITO microelectrodes. The modified electrode was integrated into a PDMS microfluidic device for *S. typhimurium* detection via electrochemical impedance spectroscopy. To minimize non-specific binding, bovine serum albumin (BSA) was injected into anti-MoS_2-NS/ITO for 5 minutes, followed by PBS wash. Then, *S. typhimurium* (80 µg/mL) was introduced for 30 minutes to promote antibody binding. This sensor achieved a detection limit of 1.56 CFU/mL across a wide range (10^1 to 10^7CFU/mL).

Jiang and colleagues developed a thread-based microfluidic electrochemical aptasensor for rapid and precise detection of Vibrio parahaemolyticus in culture media and food samples (Fig. 5a).[74] The microfluidic channel was made from threaded cotton, with nylon fiber electrodes. MoS_2-PLL-Apt conjugates were embedded onto the electrode surface, followed by incubation, washing, and BSA treatment to block active sites. After drying, pathogen binding altered the surface charge, reducing electrical flow. The aptasensor showed a broad detection range (10-10^6 CFU/mL) with an LOD ~5.74 CFU/mL, enabling faster and more accurate detection. Threaded components improved biocompatibility and preserved aptamer activity, making the sensor low-cost, portable, and suitable for clinical and food safety diagnostics.

MoS_2 has also been applied to allergen detection, such as gliadin, a dietary protein linked to allergic reaction. Traditional detection methods like ELISA and PCR have limitations, making electrochemical biosensors more practical. Ramalingam et al. developed a gliadin biosensor using a MoS_2/graphene/gold (MGG) nanocomposite (Fig. 5b).[75] Synthesized via hydrothermal and citrate

View Article Online
DOI: 10.1039/D6MA00326E

reduction, the MGG enhances electron transfer and electrochemical performance. A PDMS-based microfluidic chip with an MGG-modified electrode provides better activity and lower charge transfer resistance. The chip includes a 2 mm deep, 2 mm diameter chamber and a 75 μm wide channel. Gliadin binding reduces peak current, as shown by DPV. Optimal detection occurs at 1 μM aptamer with 10 minutes of interaction, showing linearity from 4 to 250 nM and a 7 pM LOD. The sensor accurately detected gliadin in various flours, distinguishing gluten-free from gluten-containing products.

View Article Online
DOI: 10.1039/D6MA00326E

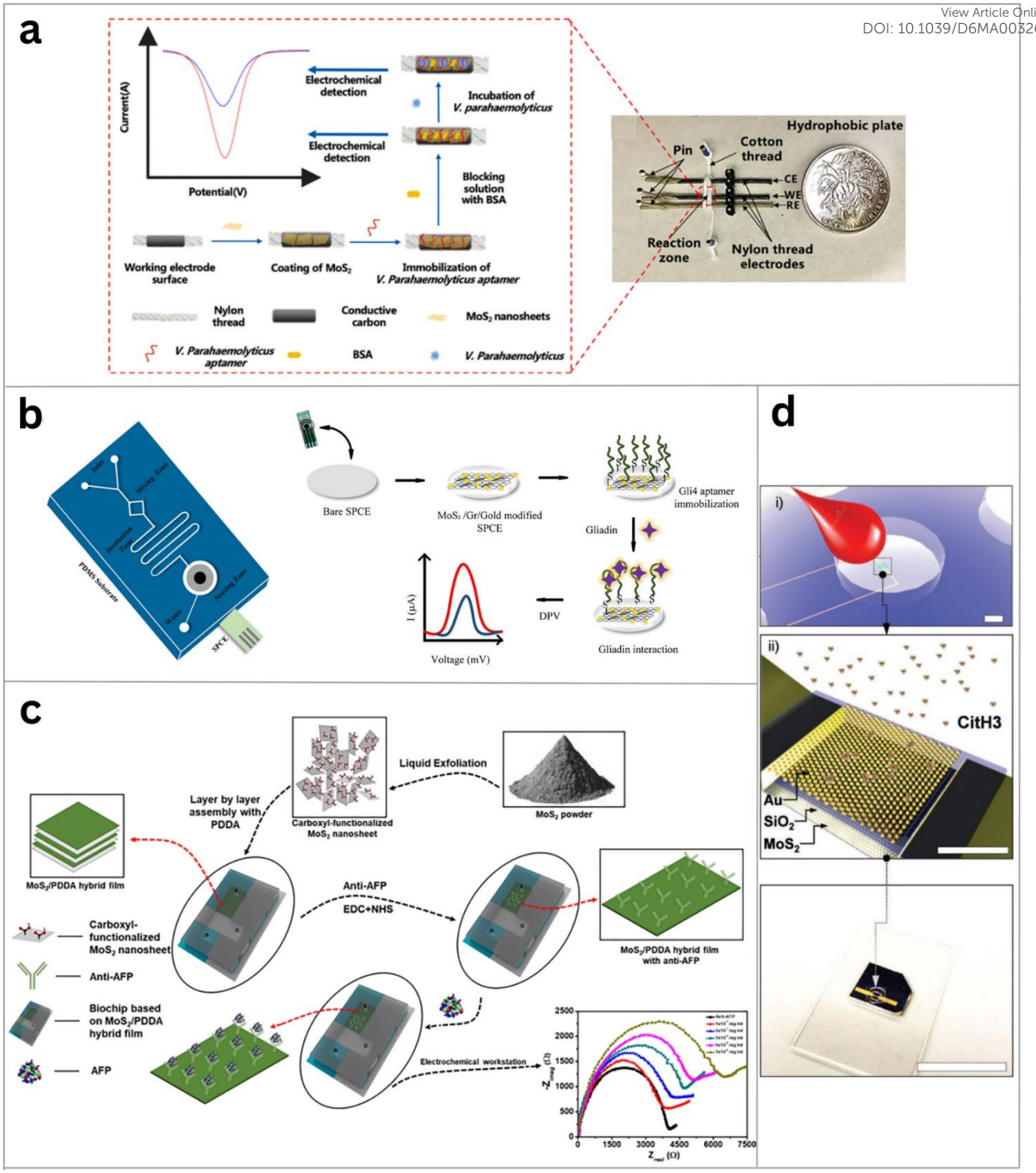

Fig. 5 MoS_2-based biosensors incorporated with microfluidic platforms for diverse bioanalytical applications: (a) Schematic of a MoS_2 modified thread-based biosensor with twisted thread electrodes forming a microfluidic network for *Vibrio parahaemolyticus* detection.[74] (b) Schematic illustration of the Gliadin sensing process using a PDMS-based microfluidic EC device.[75] (c) Structural design of a thin-core microfibre (TCMF) integrated microfluidic chip for detecting *T. gondii*.[76] (d) Illustration of the fabrication of microfluidic EC device with a self-assembled MoS_2/PDDA film and immobilized of anti-AFP for the efficient detection of alpha-fetoprotein (AFP).[77] (e) Illustration of photoconductive, few layer MoS_2 material-based NETosis-induced sepsis biomarker detecting

View Article Online
DOI: 10.1039/D6MA00326E

biosensor, including a PDMS-based microfluidic well (scale bar = 200 μm) for low-volume sample (~ 2.5 μL) consumption.[78] Adapted from Refs. 74–78 with permission.

Beyond pathogen and allergen detection, MoS_2-based biosensors hold promise in early cancer detection. Hu et al. developed a low-cost electrochemical microfluidic immunochip for detecting alpha-fetoprotein (AFP), a cancer biomarker (Fig. 5d).[77] The chip was fabricated on indium-tin-oxide (ITO) glass, etched with HCl for 150 seconds, and cleaned with acetone, isopropyl alcohol, and deionized water. A MoS_2/PDDA film was deposited on the working electrode using a layer-by-layer assembly and activated using EDC/NHS for anti-AFP immobilization. This film offered excellent conductivity and biocompatibility. The chip achieved an LOD of 0.033 ng/mL, showed high selectivity, repeatability, and retained 90% of its response after two months, proving effective for early cancer diagnosis. It showed high sensitivity, fast response, and interference resistance, ideal for point-of-care diabetic monitoring.

Another study reported a potent MoS_2-based sensitive microfluidic nano-optoelectronic biosensor (iNOBS) for monitoring CitH3, a key marker for sepsis and NETosis (Fig. 5e).[78] The device, containing gold nano hemispheres, few-layer MoS_2 photoconductive channels, and a PDMS microfluidic layer, enabled label-free detection with ultra-high sensitivity (LOD: 0.87 pg/mL), 250-fold lower than general ELISA. It offered a 20 min sample-to-answer time, high specificity, and only 2.5 μL sample use, showing strong potential for POC diagnostics.

3.1.2 $MoSe_2$-Based Microfluidic Biosensors

$MoSe_2$, a member of the TMD family, has been less explored than MoS_2 but still holds significant potential for microfluidic biosensing applications. One notable study by Sharma et al. developed a hybrid $MoSe_2$/P3HT Bio-FET device for detecting ammonia in human saliva and plasma.[79] The device showed excellent sensitivity and a low limit of detection (0.65 μM), although it did not yet incorporate a microfluidic system. The hybrid nature of the sensor, combining inorganic $MoSe_2$ and

View Article Online
DOI: 10.1039/D6MA00326E

organic P3HT, could be extended to microfluidic devices for improved performance in real-time clinical diagnostics.

3.1.3 WS_2-Based Microfluidic Biosensors

Toh and colleagues developed electrochemical microfluidic devices using TMDs like MoS_2, $MoSe_2$, WS_2, and WSe_2, exfoliated via tert-butyllithium.[80] Exfoliated TMDs were stirred at 25 °C, dispersed in water, and ultrasonicated to maintain conductivity below 20 µS. Among them, 1T-phase WS_2-based lab-on-a-chip (LOC) devices demonstrated the highest efficiency for H_2O_2 detection. PDMS microfluidic chips with 49 µm deep channels were plasma-bonded over electrodes on a glass substrate (Ag/AgCl reference electrode). H_2O_2 detection was done by injecting PBS buffer at 40 µL/min through Y-connector inlets, with H_2O_2 introduces via a separate inlet. The WS_2-based LOC device demonstrated excellent performance and selectivity in diluted human serum, with a 2.0 nM LOD.

3.2 MXene-Based Microfluidic Biosensors

Liu et al. developed a MXene-based electrochemical microfluidic chip for simultaneous detection of creatinine, uric acid (UA), and urea in whole blood (Fig. 6a).[81] The four layer-chip, made with PMMA, features a 1 mm wide, 0.5 mm deep winding channel (Fig. 6a). Whole blood enters from the top, and small molecules pass through a dialysis membrane to the detection chamber with a MXene-modified screen-printed electrode (SPE). A ratiometric sensing method using methylene blue (MB) enhances UA detection. Urea detection relies on urease-induced pH changes, while creatinine is detected via its reaction with copper ions and MXene's electrostatic adsorption. Optimized with 30 µg MXene, the sensor achieves high electrocatalytic activity. Square wave voltammetry enables signal measurement. It operates at 30 µL/min with 48-50% dialysis efficiency. The chip shows

View Article Online
DOI: 10.1039/D6MA00326E

linearity for UA (30-500 μM), urea (0-3 mM) and creatinine (10-400 μM) with LODs of 5 μM (UA) and 1.2 μM (creatinine).

In addition to multi-biomarker detection, MXene-based microfluidic platforms have the potential to detect disease markers, as demonstrated by Zhao et al. in their development of a microfluidic electrochemical platform for the sensitive detection of carcinoembryonic antigen (CEA), a tumor marker (Fig. 6b).[82] A commercially available screen-printed carbon electrode (SPCE) was modified with a novel nanocomposite, hemin-coated carboxylic carbon nanotube-decorated Ti_3C_2 nanosheets (He@CCNT/Ti_3C_2), to enhance conductivity and signal amplification. The electrode surface was further functionalized with a solution of phosphate-buffered saline (PBS) containing 0.4 M EDC and 0.2 M NHS to activate the carboxylic groups, to which aptamers were attached. Unspecific binding sites were blocked using bovine serum albumin. This biofunctionalized electrode was positioned at the bottom layer of a two-layer microfluidic chip, with a fluid channel in the top layer (1 mm × 480 μm) featuring a herringbone structure to ensure perfect mixing and transfer of CEA to the binding sites on the electrode.

View Article Online
DOI: 10.1039/D6MA00326E

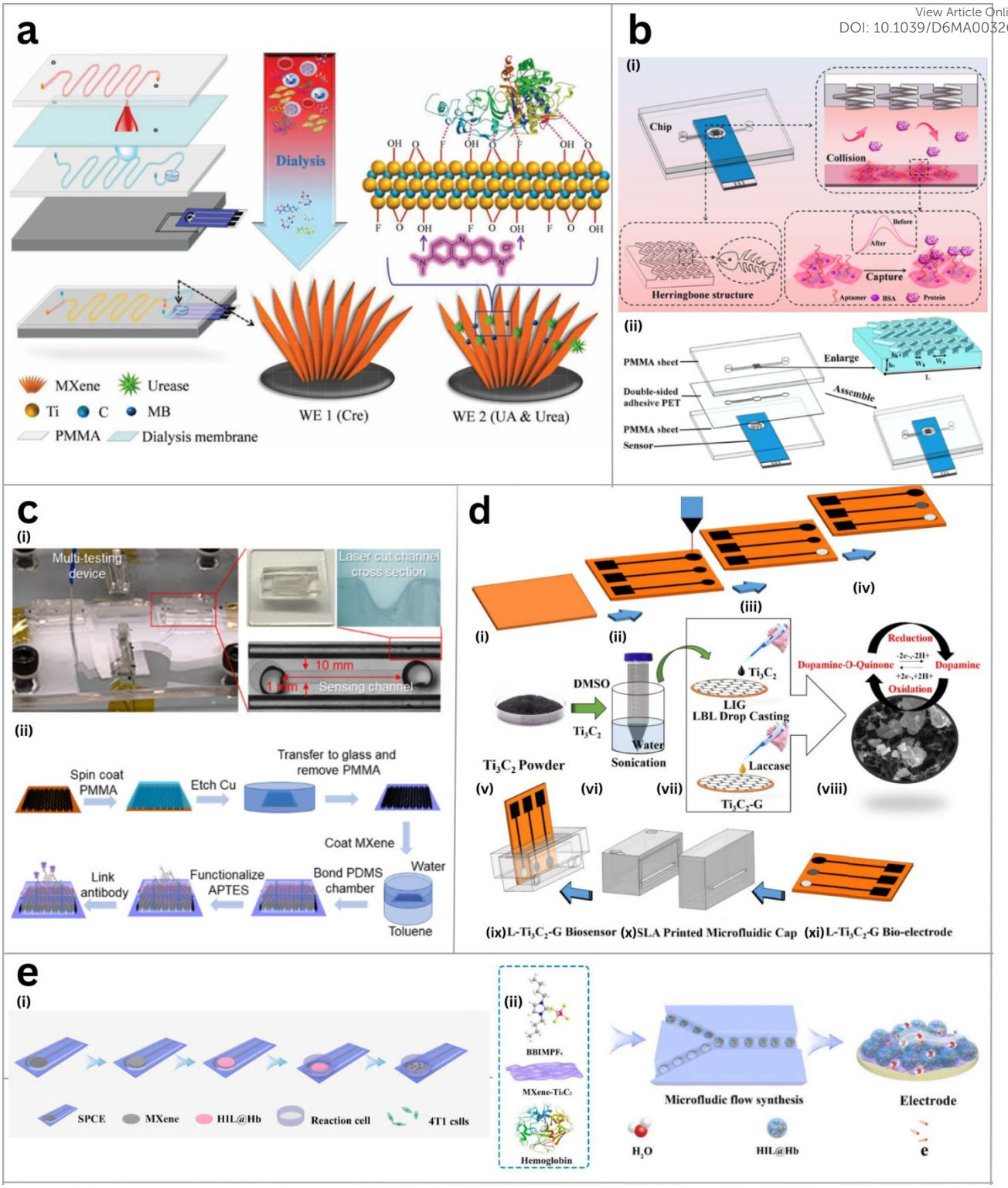

Fig. 6 MXene-based electrochemical microfluidic biosensors: (a) Schematic of a microfluidic chip integrated with MXene for simultaneous detection of urea, uric acid, and creatinine in whole blood.[81] (b) Schematic of a microfluidic chip designed for electrochemical detection of carcinoembryonic antigen (CEA) using a Ti_3C_2 MXene-based composite.[82] (c) Fabrication of microfluidic MXene–graphene sensor for parallel influenza and coronavirus detection.[83] (d) Design flow of a dopamine biosensor consisting of L-Ti_3C_2-G (LIG) composite-based bioelectrode in SLA-printed microfluidic

View Article Online
DOI: 10.1039/D6MA00326E

cap.[84] (e) Fabrication of a MXene assisted SPCE working electrode for H_2O_2 detection, along with the corresponding microfluidic flow synthesis of HIL@Hb active layer for sequential biosensing.[85] Adapted from Refs. 81–85 with permission.

The two layers were sealed using a poly(ethylene terephthalate) (PET) double-sided adhesive sheet. An insulating protein layer forms when CEA binds to the aptamers on the electrode surface, blocking electron transfer and reducing the current signal. Differential pulse voltammetry (DPV) was used to measure the electrochemical binding, showing a linear sensor response between 10 and 10^6 pg/mL, with a limit of detection (LOD) of 2.88 pg/mL. An analysis of the maximum drag force (FD) exerted by the fluid indicated that at an elevated flow velocity of 800 µL/min, the stability of the aptamer-antigen binding could be adversely affected.

Li et al. developed a microfluidic MXene-graphene-based field-effect transistor (FET) sensor for the simultaneous detection of Influenza virus (H1N1) and coronavirus (SARS-CoV-2) (Fig. 6c).[83] This sensor offers a significantly faster alternative to the conventional real-time reverse transcription-polymerase chain reaction (RT-PCR) method, which typically takes over 3 hours, achieving an average response time of approximately 50 ms. The virus-sensing transduction material (VSTM) was fabricated by depositing a MXene layer onto graphene. It was then functionalized with (3-aminopropyl) triethoxysilane (APTES) to enable subsequent antibody immobilization.

The VSTM was placed between source and drain electrodes, and a polydimethylsiloxane (PDMS) microfluidic channel with dimensions of 1 mm in length and 10 mm in width was integrated with the VSTM. Virus-specific antibodies were immobilized on the APTES-modified surface, and virus concentrations were determined by measuring the changes in the drain-source current−voltage response. The sensor exhibited outstanding sensitivity, detecting as low as 125 copies/mL for H1N1 and 1 fg/mL for SARS-CoV-2 protein, along with a broad detection range, up to 250,000 copies/mL for H1N1 and 10 pg/mL for recombinant 2019-nCoV spike protein. Despite these promising results,

View Article Online
DOI: 10.1039/D6MA00326E

the study did not report flow-based sensing of the target analytes, indicating a potential direction for future research.

Mrunali et al. developed a new microfluidic biosensor made from a composite Laccase/MXene/LIG (L-Ti_3C_2-G) using a layer-by-layer assembly for the electrochemical detection of dopamine (Fig. 6d).[84] In this design, Nafion was utilized to enable uniform coating of MXene over a densely porous graphene layer, improving conductivity and stability. The Laccase enzyme solution was drop-cast on top of MXene in order to promote efficient interaction of the substrate dopamine with laccase.

The new electrode was incorporated into a 3D-printed microfluidic chip with a defined sensing area of 3 mm × 10 mm. Upon oxidizing dopamine by laccase, dopamine-o-quinone is formed, which, in turn, is reduced back to dopamine, allowing for charge transfer to the electrode surface. This mechanism of electrochemistry results in an anodic peak current by oxidation of dopamine, enabling highly sensitive dopamine detection with a limit of detection (LOD) of 0.47 nM. Square-wave voltammetry (SWV) studies showed a linear detection range of 1–103 nM, with the sensor displaying a large sensitivity of 6.37 mA. $nM^{-1}.cm^{-2}$, indicating its potential for applications in the ultrasensitive detection of dopamine.

Gao et al. reported an MXene-Ti_3C_2 microfluidic electrochemical biosensor capable of detecting hydrogen peroxide (H_2O_2) with high sensitivity and speed (Fig. 6e).[85] The biosensor is based on a glassy carbon electrode modified with haemoglobin and hydrophobic ionic liquid HIL@Hb, which ensures a strong sensing interface. Due to the high conductivity and catalytic effects of MXene, the biosensor performed impressively with an LOD of 1.996 μM, sensitivity of 52.08 $\mu A \cdot \mu M^{-1} \cdot cm^{-2}$, and a response time of 3.0 s. Most notably, the system provided real-time, in situ monitoring of H_2O_2 released by live 4T1 cancer cells, showing potential for clinical diagnostics. 2D MXene incorporates into the microfluidic biosensor increases biomolecule stability, decreases aggregation, and increases signal reliability, leading to advanced point-of-care biosensing.

View Article Online
DOI: 10.1039/D6MA00326E

3.3 Phosphorene-Based Microfluidic Biosensors

Phosphorene, a two-dimensional form of black phosphorus, possesses high stability, a unique hinge structure, a thickness-dependent band gap, high chemical adsorption energy, abundant adsorption sites, strong in-plane anisotropy, and a reactive edge structure. These properties indicate high hole mobility and highlight the suitability of phosphorene for electrochemical biosensing applications.[86,87]

Ramalingam et al. developed a nanocomposite-based electrochemical microfluidic aptasensor for the detection of okadaic acid. The surface of bare screen-printed carbon electrodes (SPCE) was modified by drop-casting a phosphorene-gold nanocomposite along with varying concentrations of aptamers specific to okadaic acid (OA). Potassium ferrocyanide-ferricyanide was utilized as the redox pair to quantify electrochemical signals. A simple Y-channel continuous-flow microfluidic setup was fabricated, featuring a 200 μm-wide channel and a 4 mm diameter sensing zone. The system included specific zones for on-chip functions such as incubation, mixing, and sensing, designed for point-of-care analysis. The binding of okadaic acid to the sensor surface was studied via Differential Pulse Voltammetry (DPV), revealing a detection limit of 8 pM, with a linear range between 10 nM and 250 nM. The aptasensor exhibited no cross-reactivity with other food toxins, indicating that it is a convenient, point-of-care device with great potential for use in on-site assays.[88]

3.4 Paper-Based Microfluidic Biosensors

In paper-based microfluidic devices, enabling capillary flow of liquids on cellulose paper eliminates the need for pumps, making the system cost-effective and portable for on-site detection while constructing paper-based electrodes. Folding and designing papers into new shapes, assisting advanced geometry and architecture, is known as Origami, which is a new trend-setting inclusion for the modification of paper-based electrodes.

Zhang et al. fabricated a multilayered, folding origami dual-mode aptasensor integrated with microfluidic channels, electrode modification, cleaning, and dual-signal output components to detect

View Article Online
DOI: 10.1039/D6MA00326E

Ochratoxin A (OTA) food contaminants (Fig. 7a).[89] Through electrostatic interaction, chitosan-functionalized MoS_2 nanosheets (Ch-MoS_2 NS) were developed with Au@Pt nanoparticles. The authors prepared and utilized a composite (Ch-MoS_2-Au@Pt) based on the synergism between the unique raspberry-like morphology of Au@Pt NPs and the redox activity of Mo centres, which exhibited exceptional catalytic activity and acted as a mimetic enzyme for signal amplification. After each modification, bovine serum albumin (BSA) was used to block nonspecific bindings.

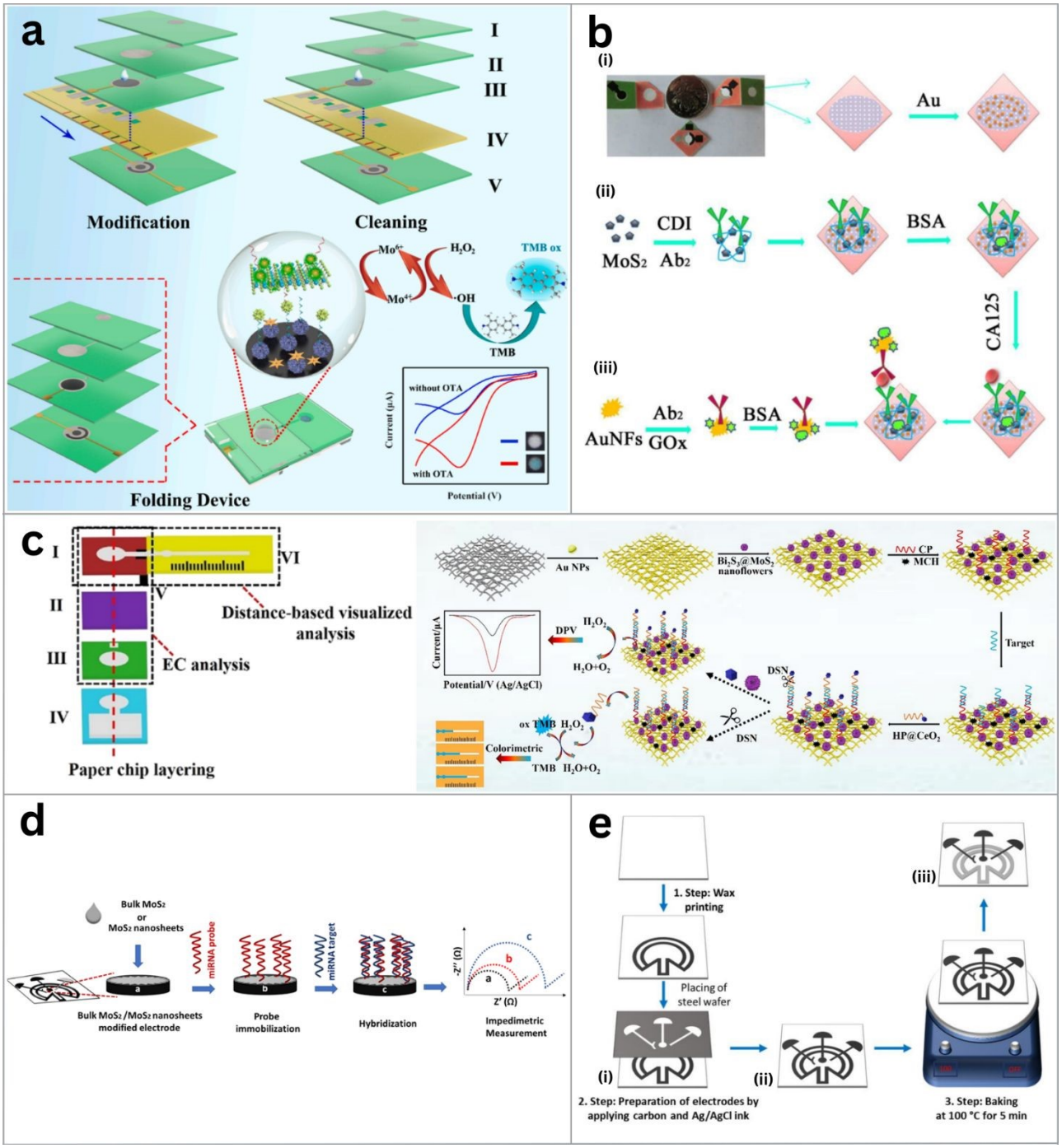

View Article Online
DOI: 10.1039/D6MA00326E

Fig. 7 Paper-based MoS_2-integrated microfluidic biosensors for bioanalytical detection. (a) Schematic of a multilayer folding origami microfluidic biosensor illustrating the OTA sensing mechanism using Ch-MoS_2 nanosheets on an EC/colorimetric PAD.[89] (b) Fabrication flow of a paper-based Au-modified working electrode (Au-PWE) integrated into a 3D origami biosensor for sensitive CA125 detection.[90] (c) Representation of a dual-mode paper-based biosensor using Bi_2S_3@MoS_2–CeO_2 on Au-μPAD for electrochemical and distance-based miRNA-141 detection.[91] (d) Illustration of a MoS_2 nanosheet-modified electrode for a paper-based specific miRNA biomarkers detection.[92] (e) Schematic of a paper-based electrochemical biosensor for miRNA detection, featuring a 0.6 cm capillary flow channel and AuNP-deposited MoS_2 electrode.[93] Adapted from Refs. 89–93 with permission.

The electrochemical signal was enhanced by the addition of OTA, which formed a sandwich complex (Ch-MoS_2-Au@Pt-apta$_2$/OTA/apta$_1$) that effectively catalyzed H_2O_2 on the sensing interface. Additionally, a colorimetric method was established, as the abundant ·OH radicals induced a visible color change by oxidizing 3,3′,5,5′-tetramethylbenzidine (TMB). This dual-mode detection method achieved limits of detection (LOD) of 1×10^{-4} ng/mL and 0.1 ng/mL for electrochemical and visual detection, respectively.

Wang et al. developed a paper electrode-based biosensor for the detection of cancer antigen 125 (Fig. 7b).[90] In this study, two types of conjugates were prepared: MoS_2-Ab$_1$, in which primary antibody (Ab$_1$) was bound to MoS_2 nanosheets by CDI linking and AuNFs-Ab$_2$, in which secondary antibody (Ab$_2$) was incorporated in AuNF suspension followed by GO_X adsorption on AuNFs. Then these conjugates were allowed to bind the sensitive wax-patterned cellulose surface pre-modified with interconnecting electrochemically active AuNP by designing a 3D origami paper-based electrochemical immunosensor. BSA was vital for preventing nonspecific binding in both conjugates. In the presence of glucose, GO_X catalyzed the oxidation of glucose to gluconic acid and H_2O_2, with the latter subsequently oxidizing the MoS_2 nanosheets and yielding DPV signals that were proportional to the concentration of the sample. This technique reached a limit of detection of 0.36 pg/mL.

Zhou et al. designed a foldable multilayer μPAD for electrochemical and visual dual-mode detection of miRNA-141 (Fig. 7c).[91] By leveraging the catalytic activities of Bi_2S_3@MoS_2 nanoflowers and

View Article Online
DOI: 10.1039/D6MA00326E

octahedral CeO_2 nanoparticles, the authors enhanced the reduction of H_2O_2, leading to a significant improvement in electrochemical analysis. Due to capillary action, excess H_2O_2 solution and released CeO_2 probes flowed to the color channel, where the oxidation of TMD produced a distinct blue visual band. The limits of detection (LODs) for the optical and electrochemical methods were determined to be 0.12 fM and 2.65 fM, respectively.

Papakonstantinou et al. designed a MoS_2-modified paper-based biosensor to investigate differences in the detection performance of miRNA-155 and miRNA-21(Fig. 7d).[92] A wax-patterned nitrocellulose (NC) membrane with a specific architecture was designed, incorporating a fluidic channel (length: 0.6 cm, diameter: 1.5 cm) that terminated in an electrochemical reaction cell with a surface area of 20 mm^2. Subsequently, all three electrodes, i.e. reference electrode (Ag/AgCl ink), working electrode, and counter electrode (both carbon paste-printed) were fabricated on the NC membrane to form a paper-based electrode modified with MoS_2 nanosheets.

Next, DNA probes specific to miRNA-155 and miRNA-21 were immobilized for 10 minutes, followed by a phosphate-buffered saline (PBS) wash to minimize non-specific binding. This method demonstrated limits of detection (LODs) ranging from 1.0 to 200.0 ng/mL for miRNA-21 and miRNA-155, while also offering high sensitivity, low sample consumption (5 µL), cost-effectiveness, and time efficiency, as the entire assay was completed in just 30 minutes.

Instead of MoS_2 nanosheets modification, gold nanoparticle nanohybrids as AuNP/RGO-modified and AuNPs/MoS_2-modified paper electrode were also fabricated for DPV detection of miRNA-155 and miRNA-21 on another approach carried out by the same group (Fig. 7e).[93] In which the LODs were found to be 12.0 and 25.7 nM for AuNPs/RGO and 51.6 and 59.6 nM for AuNPs/MoS_2 for miRNA-21 and miRNA-155 respectively.

3.5 Wearable Microfluidic Biosensor

View Article Online
DOI: 10.1039/D6MA00326E

Wearable biosensors are the portable devices which provide a simple and non-invasive solution for monitoring biological signals such as glucose level, heart rate, and composition of sweat. These sensors are commonly integrated with novel materials such as 2D nanomaterials, microfluidics, and functionalized flexible electronics, which increase their capabilities for continuous monitoring. Wearable biosensors have numerous applications, including personalized medical care, fitness performance monitoring, and disease control and prevention. By allowing real-time data collection and remote monitoring, these devices have the ability to improve health outcomes greatly.

Sweat is an extraordinary biofluid that provides valuable insights into various physiological conditions. The Park group fabricated a wearable electrochemical immunosensor integrated with a microfluidic channel for the detection of the cortisol biomarker in human sweat (Fig. 8a).[94] Immunosensors with integrated microfluidic platforms are particularly suited for cortisol measurement due to minimal contamination risk, rapid sampling, and reduced patient sample requirements. This group addressed existing limitations by utilizing laser-burned graphene (LBG), known for its straightforward production process and excellent electrochemical properties. To overcome the low resilience of LBG in biological applications, highly conductive LBG-based MXene flakes were incorporated into the electrode system. A PDMS microfluidic system was fabricated by curing a 10:1 mixture of base solution and curing agent. LBG was grown on polyimide film and transferred onto PDMS. The LBG surface was modified with MXene, followed by cortisol antibodies and BSA for surface passivation. Integrated with PDMS microchannel, the electrode formed a wearable skin patch. Electrochemical impedance spectroscopy confirmed sensor performance with a detection range of 0.01–100 nM and a limit of 88 pM, showing high selectivity and repeatability.

View Article Online
DOI: 10.1039/D6MA00326E

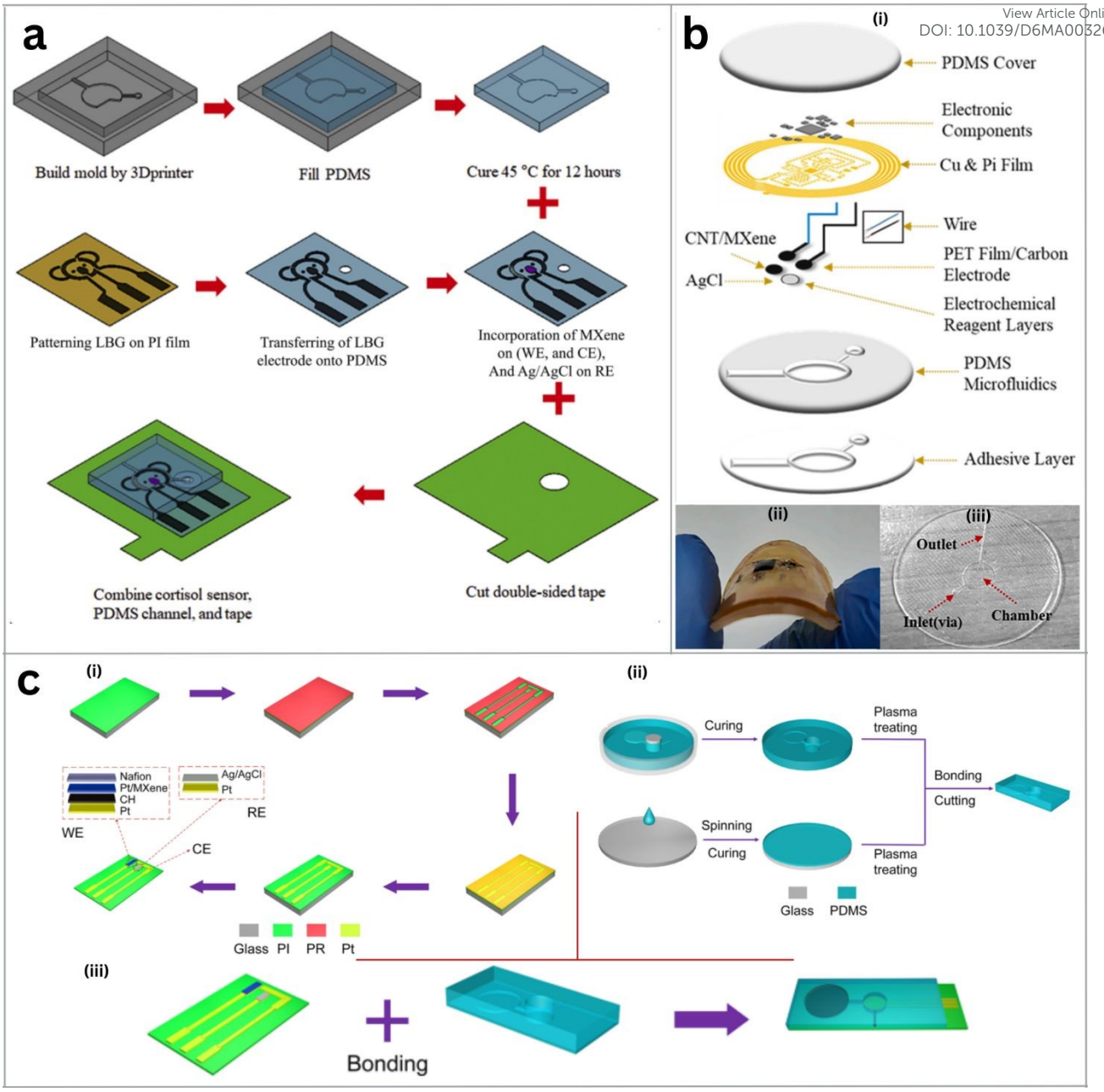

Fig. 8 Schematic representations of MXene-based wearable microfluidic biosensors: (a) Fabrication of a sensitive wearable device using MXene-LBG 3D electrodes on a PDMS microfluidic channel for cortisol detection in sweat.[94] (b) Development of a wireless, battery-free Microfluidic electrochemical (EC) device with MXene-MWCNT electrodes for K^+ detection in sweat.[95] (c) Fabrication of a flexible microfluidic biosensor integrating Pt/MXene nanomaterials with a two-partitioned microfluidic patch design for in situ glucose monitoring.[96] Adapted from Refs. 94–96 with permission.

View Article Online
DOI: 10.1039/D6MA00326E

The same research group also developed a wireless, battery-free, wearable electrochemical sensing patch system for analysing potassium ion concentrations [K^+] in human sweat (Fig. 8b).[95] In this design, they modified the working electrode using the "bridging" effect of highly conductive multiwalled carbon nanotubes (MWCNT) inserted into the $Ti_3C_2T_X$ MXenes layers to improve ion transport. On a PET substrate, the reference electrode was fabricated by drop-casting Ag/AgCl. Valinomycin as [K^+] selective carrier was also coated on the electrode for better selectivity. Sweat transport from the skin was carried through the microfluidic channel made of PDMS. To achieve cost-effective, on-site detection, a Near Field Communication (NFC) wireless patch system was used to transmit measurements to a smartphone, which also acted as an RF power source. During on-body sweat testing while cycling, the sensor detected ion concentrations ranging from 1 to 32 mM. By changing the ion-selective membranes, the sensors show high potential for detecting other biomarkers.

Electrochemical wearable biosensors are widely used for glucose detection in sweat, providing critical real-time monitoring for diabetes management. However, existing sensors face challenges: glucose catalysis issues due to direct skin adhesion and sweat accumulation beneath the sensor, which hampers efficiency. To address this, researchers developed a flexible, wearable electrochemical sensor for continuous, non-enzymatic monitoring, synthesizing Pt/MXene nanomaterials in situ by coupling Pt nanoparticles with MXene nanosheets (Fig. 8c).[96]

The sensor showed a linear detection range from 0 to 8 mmol/L. Stability was enhanced by embedding Pt/MXene in a conductive hydrogel matrix. A two-compartment microfluidic patch efficiency collected and directed sweat to the sensor. Human testing throughout the day demonstrated glucose level fluctuations reflecting energy balance changes. Validation against commercial blood glucose measurements showed comparable trends. The developed sensor offers reliable, real-time glucose monitoring, holding great promise for diabetes management.

View Article Online
DOI: 10.1039/D6MA00326E

Lei et al. fabricated a wearable multifunctional biosensing system for monitoring glucose and lactate in sweat using a novel composite MXene/Prussian blue (Ti_3C_2Tx/PB).[97] The device is based on a solid–liquid–air three-phase interface and incorporates replaceable modules to facilitate the replacement of damaged or expired electrodes in the sensor platform. The integration of the system is conducted with three modules: a sweat-uptake layer (Serpentine microfluidic tunnel) that collects sweat from the skin, a sensor layer (glucose, lactate, and pH sensors), and a cover layer (made of soft silicone rubber) with two air holes of 3 mm in diameter created via laser etching, for the free diffusion of oxygen to the active layer. To form a stable liquid-metal microwire, Galinstan (liquid-metal alloy) was injected into the serpentine microfluidic channels after assembling the sensor layer and cover layer (Fig. 9a). The width of the serpentine channels was 0.8 mm for both layers. The oxygen-rich glucose and lactate sensors were fabricated by drop-casting onto CNTs/Ti_3C_2Tx/PB modified carbon fibre microelectrodes (CFMs), with Ag/AgCl serving as the reference electrode.

Furthermore, A pH sensor was also employed to monitor local pH values. With efficient sweat collection and prolonged service life, this device showed electrochemical sensitivity of 35.3 $\mu A mm^{-1} cm^{-2}$ for glucose and 11.4 $\mu A mm^{-1} cm^{-2}$ for lactate, demonstrating the high potential of MXene-based composites in wearable microfluidic biosensing applications.

View Article Online
DOI: 10.1039/D6MA00326E

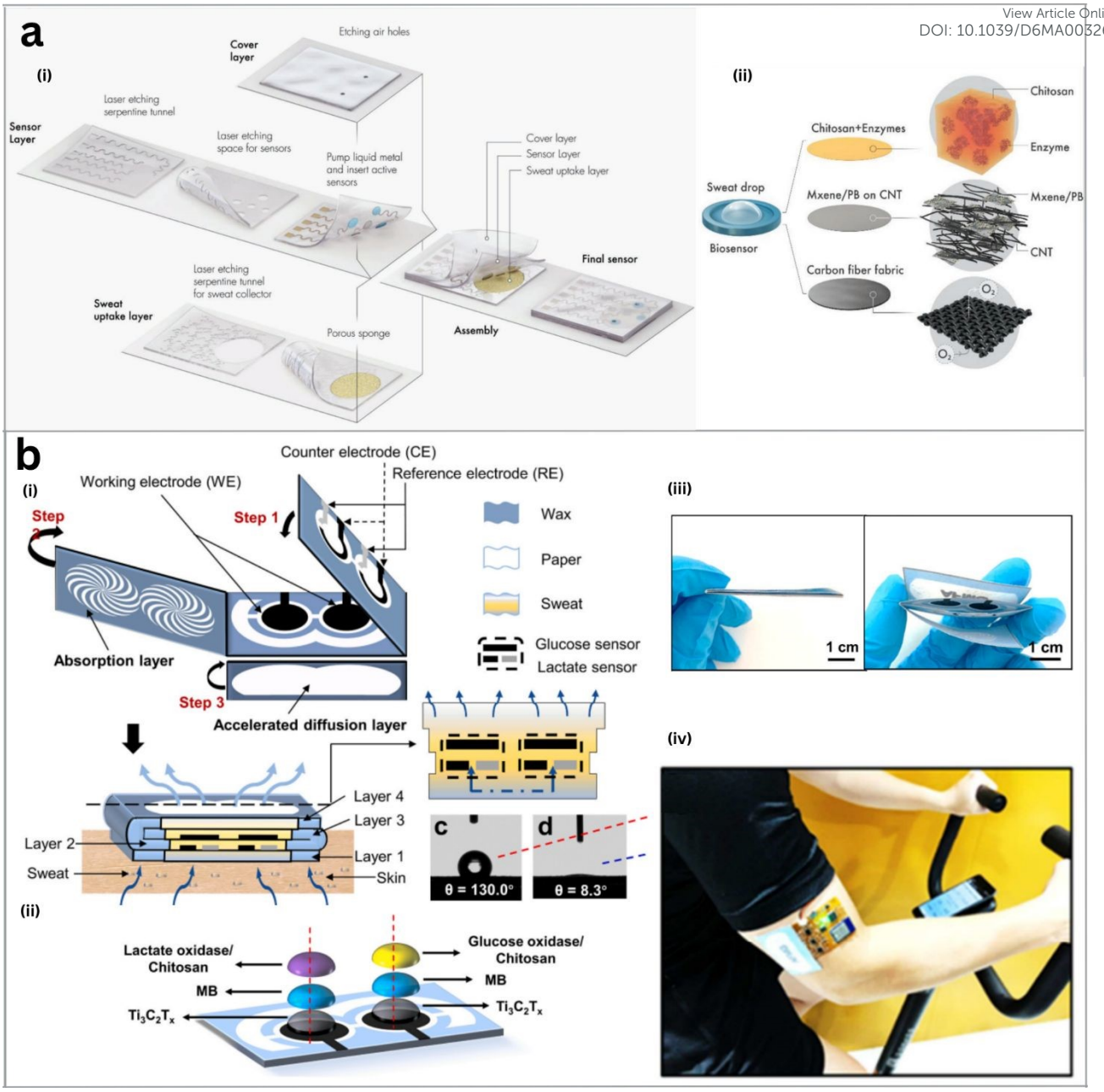

Fig. 9 Fabrication details of wearable sweat-sensing biosensors: (a) Schematic of a wearable sweat-sensing biosensor consisting of a serpentine microwire prepared by injecting a metal alloy through a microfluidic channel.[97] (b) Illustration of the structural details of a foldable microfluidic HIS paper and fabrication of working electrodes for glucose and lactate detection in sweat. (ii, iii) Exploded view of the foldable HIS paper.[98] Adapted from Refs. 97–98 with permission.

Li et al. designed a foldable, highly integrated, multilayer paper-based (HIS paper) wearable sensor for the detection of lactate and glucose in sweat (Fig. 9b).[98] Four layers, each with an area of 19.25

View Article Online
DOI: 10.1039/D6MA00326E

cm^2 (35 mm × 55 mm), and specific functions, were printed on the paper substrate and folded into a 3D structure to diffuse sweat to the electrodes efficiently using capillary flow. The major sensing interface single-layer structure was fabricated with $Ti_3C_2T_X$ followed by methylene blue (MB) modification for biomolecule immobilization. This wearable sensor resulted in 2.4 nAμM^{-1} for glucose and 0.49 μAmM^{-1} for lactate in human sweat analysis.

Beyond glucose and lactate, other biomarkers such as uric acid and oxidative stress indicators have also been targeted using MXene-based wearable biosensors. Luo et al. built a biofouling-resistant wearable electrochemical sensor to detect uric acid (UA) and ascorbic acid (AA) in real sweat.[99] Harnessing the excellent flexibility, water tolerance, and large specific surface areas of hydrogels, the authors created a soft electronic skin to form a network structure and carried abundant hydrophilic groups resulting in AuNPs/MoS_2/Pep hydrogel. An anti-fouling membrane was introduced to reduce nonspecific adhesion by precisely controlling −COOH and −NH_2 groups in the peptide. In this design, MoS_2 contributed self-healing properties by the binding force of π−π stacking between MoS_2 and naphthalene groups (Nap-peptide) as well as MoS_2AuNPs/ MoS_2.

View Article Online
DOI: 10.1039/D6MA00326E

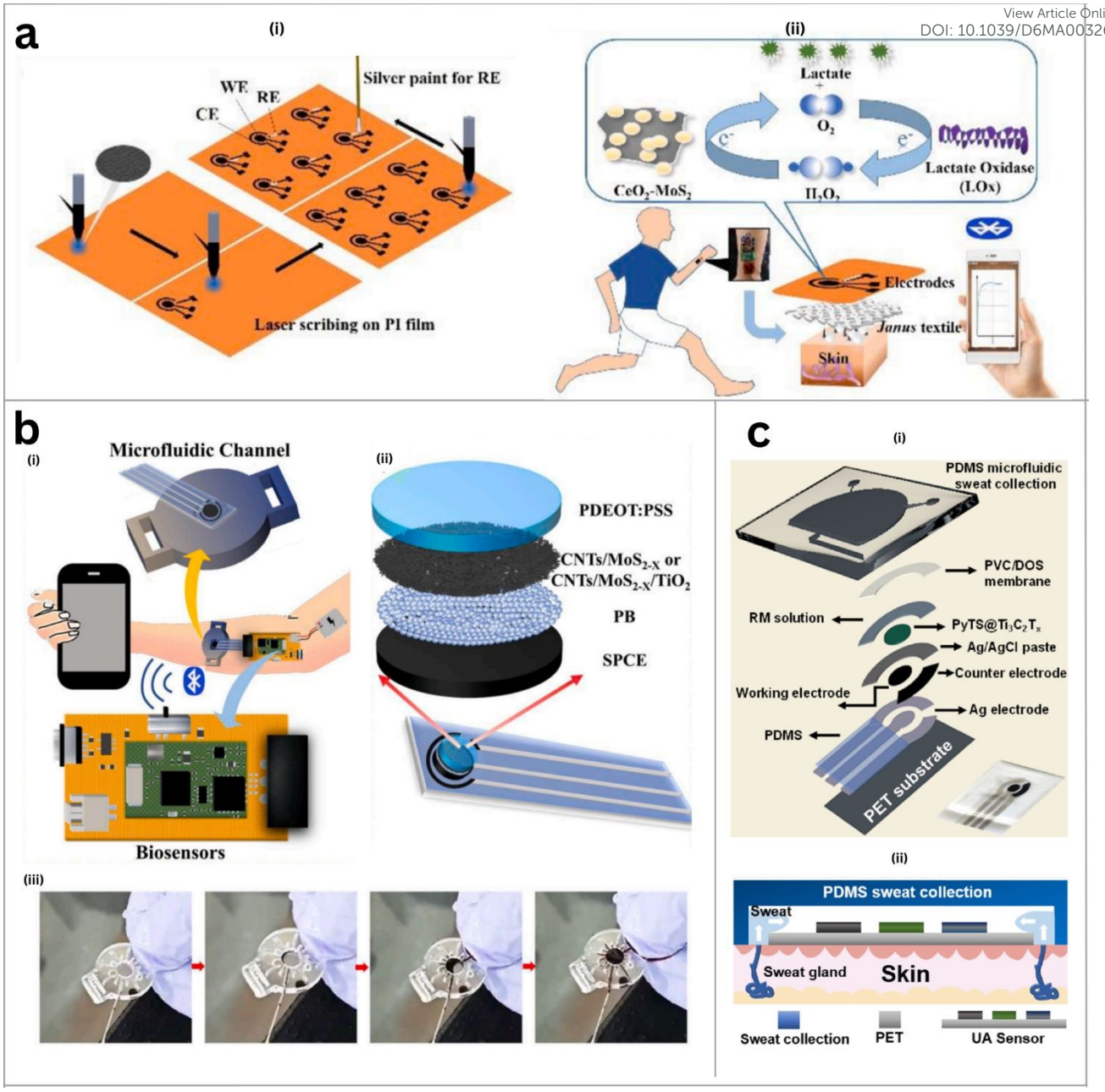

Fig. 10 (a) Lactate monitoring wearable biosensor: (i) Fabrication of a three-electrode setup via laser scribing on a thin PI film. (ii) Real-time electrochemical interaction of lactate in sweat using a CeO_2-MoS_2 nanozyme-based sensing material.[100] (b) Non-invasive stress biomarker detection biosensor: (i) Integrated microfluidic channel for sweat analysis. (ii) Exploded view of the MoS_2-X-based sensing electrode.[101] (c) Integration of a wearable PyTS@Ti3C2Tx-based microfluidic chip and illustration of sweat collection for monitoring uric acid (UA) metabolites.[102] Adapted from Refs. 100–102 with permission.

View Article Online
DOI: 10.1039/D6MA00326E

Jiang et al. developed a wearable nanozyme-enzyme electrochemical nanobiosensor for monitoring lactate level in sweat (Fig. 10a).[100] To facilitate directional sweat transportation, a flexible laser-scribed graphene (LSG) electrode and a Janus textile made of cotton and Ecoflex were prepared on a polyimide (PI) film. MoS_2 nanoflakes were synthesized through an exfoliation process to synthesize CeO_2- MoS_2 nanozyme, which enabled co-catalytic activity. This nanozyme was then drop-casted on the working electrode and electrodeposited with gold nanoparticles (AuNPs) for the enhancement of electrochemical signals by H_2O_2 reduction. A three-electrode system consisting of a CeO_2 MoS_2/Au/LOx modified working electrode (WE), a graphene counter electrode (CE), and an Ag/AgCl reference electrode (RE) was incorporated into the sensing device. The biosensor can perform a single lactate test in just 2 min at a very low cost. This method has shown a limit of detection (LOD) down to 0.135 mM in artificial sweat.

Building on the concept of sweat monitoring, Ying et al. developed a wearable electrochemical biosensor for continuous and noninvasive monitoring of oxidative stress, focusing on hydrogen peroxide (H_2O_2) and phosphorylated proteins detection in sweat (Fig. 10b).[101] The microfluidic system was designed using OpenSCAD software and fabricated via high-precision stereolithography 3D printing (SLA) with photosensitive resin. The STL model was sliced horizontally and solidified by UV laser, creating an intricate microfluidic channel with a 500 μm radius and 400 μm depth, leading to a reservoir, with a concave skin contact surface for improved sweat transfer. To modify the Prussian blue working electrode, low-sulphur molybdenum disulfide was applied to multi-walled carbon nanotubes (CNT/MoS_2-X) with a coaxial core-shell structure. H_2O_2 oxidation generated an increase in current, while TiO_2-modified CNTs/MoS_2-X enabled phosphorylated protein detection by decreasing current. The sulphur vacancy-enhanced coaxial structure significantly improved sensitivity. The sensor achieved detection limits of 4.80 μM for H_2O_2 and 0.917 μg/mL for phosphoproteins.

View Article Online
DOI: 10.1039/D6MA00326E

Chen et al. developed a wearable microfluidic biosensor functionalized with MXene for the real-time monitoring of uric acid (UA) metabolites in sweat (Fig. 10c).[102] The device was fabricated by screen-printing flexible electrodes onto a transparent polyethylene terephthalate (PET) membrane. MXene nanosheets were modified with 1,3,6,8-pyrenetetrasulfonic acid sodium salt (PyTS), a bifunctional molecule, via π-π conjugation to form a UA-selective membrane that was applied to the working electrode. To prevent short-circuiting, a polydimethylsiloxane (PDMS) layer covered all but three electrodes of the conductive substrate. The sensing electrodes were integrated into a microfluidic chip designed for sweat collection, transport, and ejection. Upon contact with the electrode surface, UA in sweat underwent electrochemical oxidation via a two-electron/two-proton redox reaction. This generated an oxidation peak, which allowed the quantification of UA in sweat. The device demonstrated high selectivity for UA over other metabolites, such as glucose and lactic acid, with a limit of detection (LOD) of 0.48 μM. However, slight interference in current response was observed in the presence of CO_2. The authors also reported a strong correlation between UA levels in sweat and blood.

Extending wearable biosensing into ocular fluids, Shiqi Guo et al. developed a microfluidic FET-based smart contact lens for human tear fluid analysis, with multifunctional sensing capabilities, including MoS_2 photodetection, glucose detection, and temperature detection. The ultrathin MoS_2 sensor was transferred onto a PDMS substrate to create a soft, biocompatible, and non-toxic smart contact lens. This highlights its potential for ocular disease research and future wearable diagnostic applications.[103]

Table 2: Electrochemical microfluidic biosensors.

Target/Analyte	2D material Used	Detection Principle	Sensor Format	LOD	Linear range	reference
BPA	MoS_2	FET	PDMS	1 pg/mL	1 pg/mL –1 μg/mL	[65]

View Article Online
DOI: 10.1039/D6MA00326E

TNF-α	MoS_2	FET	PDMS	60 fM	60 fM–6 pM	66
Streptavidin, IL-1β	MoS_2	FET	PDMS	~1 fM	0 – 500 fM	67
PSA	MoS_2	FET	PDMS	800fg/mL		68
Nicotine	MoS_2	FET	PDMS	-		69
Uric Acid	MoS_2	FET	PDMS	60 nM		70
DNA (trisomy 21)	MoS_2	FET	PDMS	<100 aM		71
miRNA205	MoS_2- $CuFe_2O_4$	EIS, CV, SWV	PDMS	0.48 pM	1 pM – 1.5 nM	72
Salmonella typhimurium	CTAB-MoS_2-NS	EIS	PDMS	1.56 CFU/mL	10^1–10^7 CFU/mL	73
V. parahaemolyticus	MoS_2-PLL-Apt	EIS	Thread-based	~ 5.74 CFU/ mL	10–10^6 CFU/ mL	74
Gliadin	MoS_2/Graphene/Au	DPV	PDMS	7 pM	4–250 nM	75
AFP	MoS_2/PDDA	EIS		0.033 ng/ml	1 × 10−7–1 × 10−5 mg/ml	77
CitH3	MoS_2		PDMS	0.87 pg/mL		78
NH_4^+/NH_3	$MoSe_2$	FET		0.65 µM		79
H_2O_2	WS_2	Chronoamperometry	PDMS	2.0 nM	0.02–20 µM, 0.1–2 mM	80
UA, Urea, Creatinine	MXene	CV EIS SWV	PMMA	LOD_{UA} 5 µM, LOD_{Cre} 1.2 µM	0.03–0.5 mM, 0–3 mM, 0.01–0.4mM	81
CEA	He@CCNT/Ti_3C_2	DPV	PMMA	2.88 pg/mL	10^1 –10^6 pg/mL	82
H1N1 SARS-CoV-2	$Ti_3C_2T_X$/Graphene	FET	PDMS	LOD_{H1N1} 125 copies/mL, $LOD_{SARS\text{-}CoV\text{-}2}$1 fg/mL	125–250,000 copies/mL, 1–10 pg/mL	83

View Article Online
DOI: 10.1039/D6MA00326E

Dopamine	L-Ti_3C_2-G	SWV	Polyamide Sheet	0.47 nM	1–10^3 nM	84
H_2O_2	MXene	CV		1.996 µM	1.996 µM–27.232 µM	85
Okadaic Acid	Phosphorene-Gold NC	DPV CV	PDMS	8 pM	10nM – 250nM	88
Ochratoxin A	Ch-MoS_2-Au@Pt	CV EIS Colorimetric	Paper	25.2 fg/mL	0.0001–200 ng/mL	89
CA 125	MoS_2	DPV EIS	Paper	0.36 pg/mL	0.001–50 ng/mL	90
MIRNA-141	Bi_2S_3@MoS_2nanoflowers	CV DPV EIS Colorimetry	Paper	0.12 and 2.65 fM	0.5 fM–1 nM, 10 fM–1 nM	.91
miRNA-155 miRNA-21	MoS_2	EIS	Paper	1–200 ng/mL.	0.25–0.75 µg/mL, 0.25–0.75 µg/mL	92
miRNA-155 miRNA-21	AuNPs/MoS_2	DPV CV	Paper	$LOD_{miRNA-155}$51.6 nM $LOD_{miRNA-21}$59.6 nM		93
Cortisol	$Ti_3C_2T_x$/LBG	EIS	PDMS	88 pM	0.01–100 nM	94
K^+	MWCNT/MXene	CV EIS	PET		1-32mM	95
Glucose	Pt/MXene	CV	PDMS	29.15 µM	0−8 mM	96
Glucose and Lactate	$Ti_3C_2T_x$/PB	Chronoamperometry				97
Glucose and Lactate	MXene	Chronoamperometry	Paper	17.05 µM, 3.73 µM	0.08–1.25 mM, 0.3–20.3mM	98
UA and AA	AuNPs/MoS_2/Pep hydrogel	DPV		LOD_{UA} 6.0 nM, LOD_{AA} 0.67 µM	0.00002–0.11 mM, 0.11 - 3.01 mM	99

View Article Online
DOI: 10.1039/D6MA00326E

Lactate	CeO_2–MoS_2/Au	CV	Polyimide	0.135 mM		100
H_2O_2 Phosphorylated proteins	CNT/MoS_2-X	CV DPV EIS	Resin	4.80 μM 0.917 μg/ml	0.01–1 mM, 0.01–1 mg/mL	101
UA	MXene	Chronoamperometry	PDMS	0.48 μM		102

BPA: Bisphenol A; MoS_2: Molybdenum disulfide; TNF-α: Tumor Necrosis Factor-alpha; IL-1β: Interleukin-1β; PSA: Prostate Specific Antigen; CTAB: Cetyltrimethyl Ammonium Bromide; *V. parahaemolyticus*: *Vibrio parahaemolyticus*; AFP: Alpha-fetoprotein; CitH3: Citrullinated histone H3; $MoSe_2$: Molybdenum diselenide; WS_2: Tungsten disulfide; CEA: Carcinoembryonic Antigen; OTA: Ochratoxin A; CA 125: Cancer Antigen 125; K^+: Potassium ions; MWCNT: Multiwalled Carbon Nanotubes.

4. Optical Microfluidic Biosensors

In recent years, optical biosensors have gained significant attention as a research focus. These sensors operate by utilizing light transmission and detecting optical signals. Compared to conventional electrical sensors, optical biosensors offer key advantages, including immunity to electromagnetic interference, resistance to corrosion, and exceptional sensitivity.[104] Two-dimensional (2D) materials are increasingly being integrated with microfluidic platforms for optical biosensing, reducing sample consumption and instrumentation costs while enhancing portability and sensitivity. The optical response of a 2D material to incident light, determined by their dielectric constant or complex refractive index, can be modulated by external factors like electric gating, optical fields, and thermal heating.[105,106] Changes in size and shape alter the band gap and thus affect their optical properties at the nanoscale.[107] Nanomaterials serves as sensing elements, fluorescence quenchers, labels, and waveguides in optoelectronic devices.[108]

View Article Online
DOI: 10.1039/D6MA00326E

Optically active quantum dots, often used in fluorescence-based sensing, function as fluorophores and quenchers depending on the analyte.[109] The mechanism relies on energy transfer, where fluorescence is quenched in the presence of an acceptor molecule.[110,111] The extent of quenching correlates with analyte concentration.[112] Biocompatible 2D materials can further improve fluorescence-based biosensing in bioassays.[113]

Molybdenum disulfide (MoS_2) stands out for its excellent optical properties and tunable features.[114] It can shift between low and high fluorescence states and exhibit strong light-matter interaction. In its 0D quantum dot form, MoS_2 shows high fluorescence, while the 2D nanosheet from enables effective fluorescence quenching.[115] It enhances detection techniques such as surface plasmon resonance (SPR) and fluorescence in microfluidic platforms. Other 2D materials like MXene, MBene, and g-C_3N_4 are also under investigation due to their unique optical and high biocompatibility.

4.1 Fluorescence Microfluidic Biosensors

Fluorescence-based microfluidic biosensors are powerful tools for highly sensitive and selective detection of biomolecules and metal ions. Utilizing fluorescence quenching and recovery mechanisms, and enhanced by novel 2D materials, they offer real-time, stable, and cost-effective detection, positioning them as key components in next-generation diagnostics and environmental or wearable sensing.

A fluorescence-based microfluidic biosensor using a Lys-AuNPs@MoS_2 nanocomposite has been developed for the rapid detection of cardiovascular diseases, such as acute coronary syndrome, myocardial injury, and heart failure (Fig. 11a).[116] The biosensor integrates a three-layered microfluidic chip: a PDMS sample loading layer with 60 chambers, a 50 μm wide microchannel layer, and a functional detection layer with Lys-AuNPs@MoS_2 immobilized on glass via APTES. Gold nanoparticles were electrostatically integrated onto MoS_2 nanosheets and functionalized with L-cysteine, enhancing fluorescence signal intensity, stability, and biomolecule binding efficiency.

View Article Online
DOI: 10.1039/D6MA00326E

The system requires only 2 μL of sample per chamber and achieves high selectivity via antibody-antigen binding. Fluorescence signals were collected using a GenePix 4400A laser scanner, enabling multiplexed detection. The biosensor showed excellent stability for up to 60 days, with antigen-antibody incubation saturation in 20 minutes and a total detection time of 40 minutes. Compared to conventional methods, it offers faster detection, lower reagent consumption, and higher sensitivity, successfully detecting six biomarkers in serum.

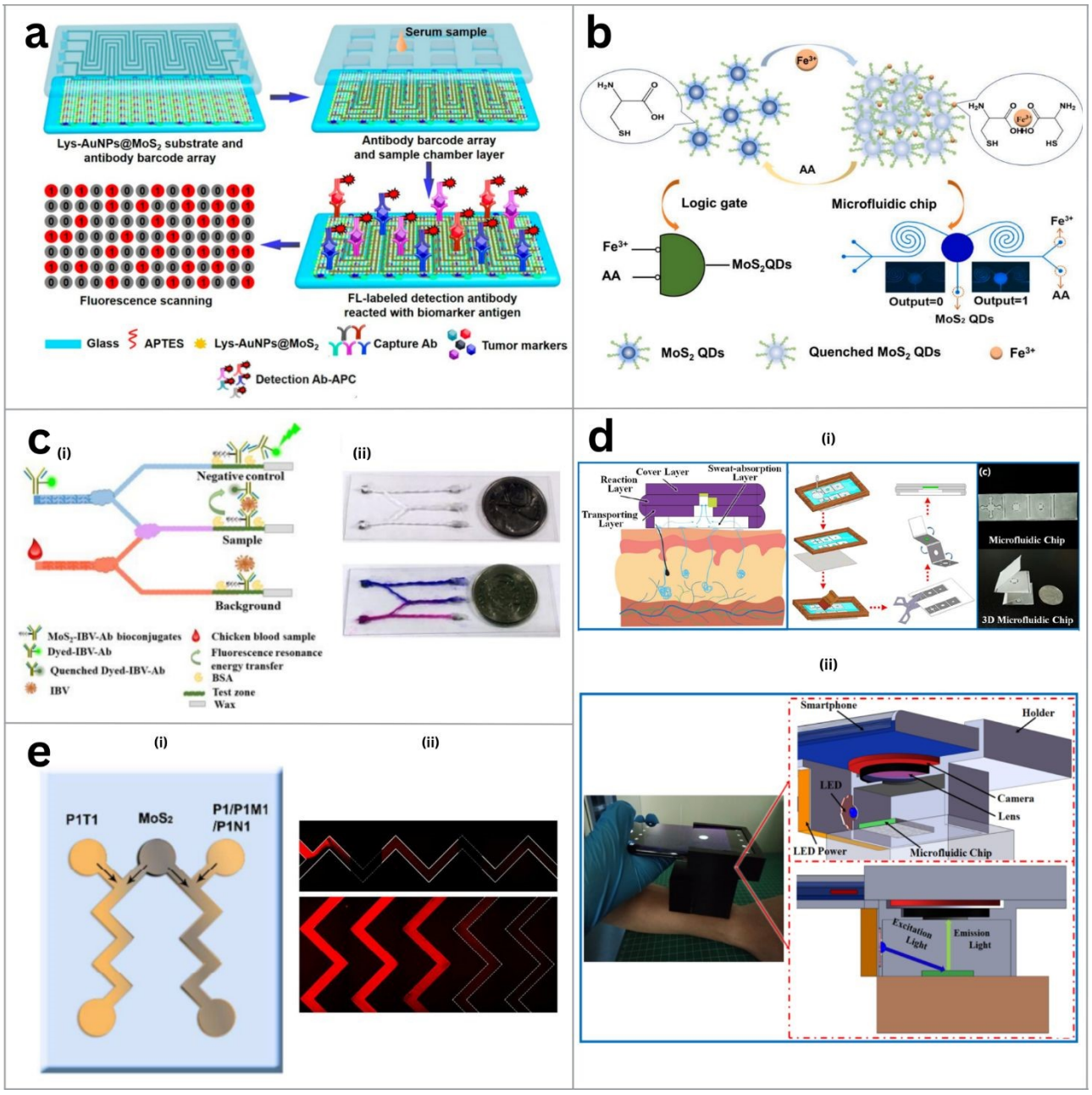

View Article Online DOI: 10.1039/D6MA00326E

Fig. 11 MoS_2-based microfluidic fluorescence biosensor: (a) Lys-AuNPs@MoS_2 with S-shaped channels for cardiovascular biomarkers.[116] (b) N-doped MoS_2 QDs for Fe^{3+}/AA detection via IMPLY logic readout.[117] (c) Thread-based FRET sensor for IBV detection.[118] (d) 3D origami chip for sweat cortisol sensing.[119] (e) DNA detection using zigzag microchannels and photoluminescence spectra.[120] Adapted from Refs. 116–120 with permission.

A notable example of this advancement is the development of fluorescence sensors based on nitrogen-doped MoS_2 quantum dots (QDs), which have been employed for the sequential detection of iron (Fe^{3+}) and ascorbic acid (AA). Zhang et al. utilized the 'visible-invisible-visible' photoluminescence property of these QDs to fabricated a dual-target fluorescence sensor (Fig. 11b).[117] Ascorbic acid reduces the reactive oxygen species (ROS) level in body by minimizing the overflow of Fe^{3+} ions. Fluorescence quenching could effectively be induced by Fe^{3+} ions. However, introduction of Ascorbic acid (AA) can recover the quenching. In microfluidic chip operation, they have injected hydrothermally synthesized nitrogen-doped MoS_2 QDs, Fe^{3+} ions and AA in three different microchannels and incubated the solution for 25 min. After that, the microfluidic chip was integrated with "IMPLY" logic gate which has utterly satisfied microliter reagent consumption, automated operation and visible readout. For this fluorescence sensor, the limit of detection were 11 μM for Fe^{3+} and 960 nM for and AA, respectively.

Fluorescence-based biosensors have also been integrated into alternative substrates, such as thread, to expand their applicability. Utilizing the wicking properties of thread, Weng et al. demonstrated a fluorescence resonance energy transfer (FRET)-based biosensor on cotton thread, incorporating antibody-functionalized MoS_2 for the detection of Infectious bronchitis virus (IBV) (Fig. 11c).[118] First, two distinct antibody (Ab) probes, MoS_2-IBV-Ab and dyed-IBV-Ab, were modified with MoS_2 and dye, respectively. Due to antigen-antibody interaction, these bioconjugates specifically bind to the target IBV. The formation of 'sandwich' complexes (dyed-IBV-Ab/IBV/MoS_2-IBV-Ab) results in successive fluorescence quenching, which correlates with increasing concentration of IBV. This method exhibited a sensitivity of 4.6×10^2 EID_{50} per mL, with a standard derivation of 1.0-10 % and

View Article Online
DOI: 10.1039/D6MA00326E

a total detection time of 10 minutes. A thread-based microfluidic device has a better mechanism over a paper-based device because of its high strength and also it does not need any hydrophobic barrier to control the fluidity of liquid.[121]

Apart from the thread-based biosensors, fluorescence biosensors have also been integrated into paper-based microfluidic systems to enhance portability and ease of use. One such example is the 3D origami biosensor developed by Jiang et al. for detecting cortisol levels in human sweat as a 'stress biomarker' (Fig. 11d).[119] A four-layer paper substrate (10 cm × 2.5 cm, l × w) with microchannels was cut and folded to create a 3D microfluidic chip. A quenching system composed of an anti-cortisol aptamer and MoS_2 nanosheets was integrated onto the paper substrate, enabling fluorescence resonance energy transfer (FRET) analysis using a smartphone. The microchannels, formed by PDMS-based hydrophobic barriers, facilitated the controlled flow of a reduced sweat sample volume (20 μL). In artificial sweat, with an analysis time of 25 minutes, this method achieved an LOD of 6.76 ng/mL.

Due to its fluorescence and quenching capabilities, MoS_2 can be utilized in biosensing applications for the detection of cancer biomarkers, DNA, and a variety of amino acids.[122,123] The strong binding affinity between the nucleic acid bases and MoS_2 has been utilized in various biosensors. Huang et al. designed multiple optical sensors integrated with microfluidic systems that utilized this binding, achieving DNA detection through the fluorescence quenching ability of MoS_2 nanosheets (Fig. 11e).[120] A dye-labelled single stranded DNA probe (P1), MoS_2 nano-sheets, and varying concentrations of complementary target DNA (T1) were employed in a PDMS-on-glass device with zigzag-shaped microchannels of 100 mm width and 40 mm depth. Interactions between P1 and MoS_2 resulted in the adsorption of P1 onto the MoS_2 surface, leading to fluorescence quenching. However, hybridization between P1 and T1 formed a double-stranded DNA structure, which, due to its lack of

View Article Online
DOI: 10.1039/D6MA00326E

affinity towards MoS_2, prevented fluorescence quenching. Maximum mixing and quenching efficiency were ensured by using high concentration of MoS_2 and slow flow rate. The calibration curve shows a linear range between 0 and 50 nM, with a LOD of 500 pM. The same group developed a MoS_2/multi-walled carbon nanotube (MWCNT) composite which showed better quenching stability than its individual components.[124] This composite retained the MoS_2 and P1 interaction principle and achieved DNA detection at 1 nM, maintaining a 0–50 nM linear range. The stable quenching performance of the MoS_2/MWCNT solution within a microfluidic setup simplifies large-scale DNA detection, making it a promising material for fluorometric biosensing.

Fluorescence-based biosensors have also been explored for diagnosing neurodegenerative diseases. Wen et al. have developed an innovative biosensor for detecting amyloid β protein oligomers (AβO), a crucial biomarker for diagnosing Alzheimer's disease (AD) (Fig. 12a).[125] This biosensor seamlessly integrated fluorescence resonance energy transfer (FRET)-based analysis with a microfluidic system crafted from poly(dimethylsiloxane) (PDMS) in a groundbreaking manner. The chip served as the detection platform and was constructed by sandwiching a PDMS microarray layer between a cover layer and a substrate glass layer. It includes around 1800 microchambers, each with a 220 μm diameter and 100 μm depth, featuring microchannels with 88 μm width and a 30 μm depth.

View Article Online
DOI: 10.1039/D6MA00326E

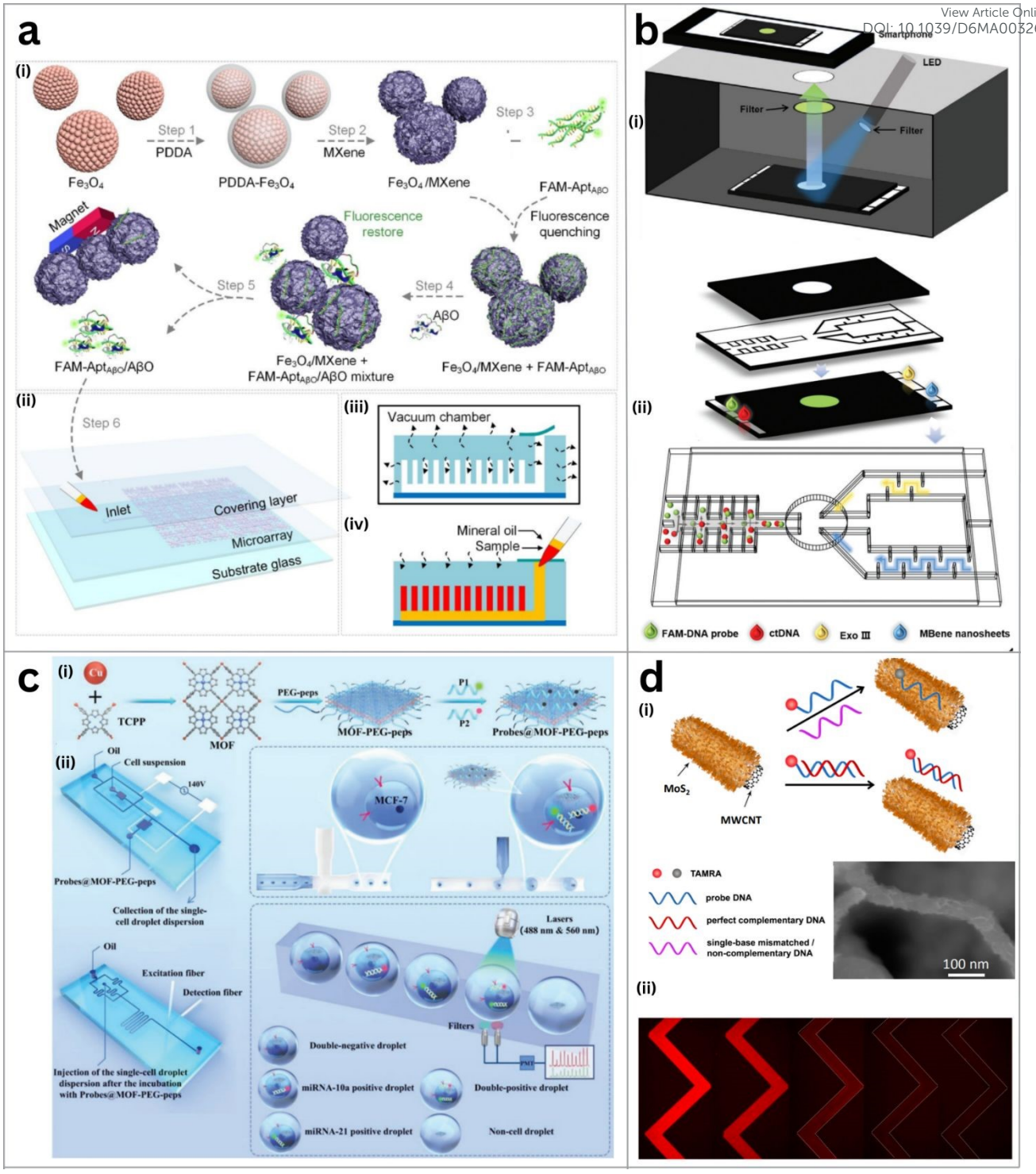

937

938 Fig. 12 Microfluidic fluorescence biosensor: (a) AβO detection using a 1792-microchamber chip
939 with sample flow driven by mineral oil.[125] (b) ctDNA sensing with FAM-DNA probe and dual-
940 channel Exo III/MBene delivery.[126] (c) MOF-PEG-peps nanosensors for miRNA detection via
941 microfluidic droplet fluorescence.[127] (d) MoS_2/MWCNT nanocomposite-based DNA sensor with
942 SEM visualization.[128] Adapted from Refs. 125–128 with permission.

View Article Online
DOI: 10.1039/D6MA00326E

The team used MXene, a 2D material with a strong fluorescence quenching effect on fluorophore-labeled DNA, to synthesize Fe_3O_4/MXene nanospheres, which played the role of fluorescence quencher in the system. Notably, this marks the first application of these elements in combination. The AβO aptamer was modified with the carboxyfluorescein (FAM) to serve as a fluorescence probe for FRET technology, which gets triggered by a specific excitation wavelength. The interaction of the modified aptamer (FAM-AptAβO) with Fe_3O_4/MXene nanospheres resulted in its adsorption on the nanomaterial surface, leading to the fluorescence quenching. However, the introduction of AβO facilitated the desorption of FAM-AptAβO from the nanosphere surface, forming FAM-AptAβO/AβO complexes through interacting with AβO, thereby restoring fluorescence.

During the detection process, a high fluorescence background or false positive signal was found due to MXene's self-fluorescence property and its inability to achieve complete fluorescence quenching efficiency. To mitigate this, magnetic separation of Fe_3O_4/MXene nanospheres from the mixture of FAM-AptAβO-Fe_3O_4/MXene and AβO was initiated. The supernatant containing FAM-AptAβO/AβO was then injected into the microfluidic chip inlet. Transportation of the sample from the inlet to the microchambers was achieved by adding mineral oil, which pushed the sample forward, and by degassing the PDMS layer, which generates sufficient negative pressure to drive the sample into the chambers. The detection showed an excellent linear relationship between fluorescence intensity and the logarithm of the AβO concentration, spanning from 0.10 to 200 nM, with an impressive detection limit of approximately 0.05 nM, utilizing only 4.50 μL of sample.

MBene, an emerging derivative of MXene, has shown great potential since its inception in 2017, particularly in the field of MXene applications, due to its specific characteristics relevant to biosensing strategies. The synthesis of MBene through an exfoliation process, by etching out A from the MAB phase, is similar to the process of etching out A from the MAX phase to obtain MXene.[129]

View Article Online
DOI: 10.1039/D6MA00326E

Yang et al. developed a paper-based microfluidic exonuclease III-assisted fluorescence biosensor for the detection of circulating tumor DNA (ctDNA) in blood samples from mice, utilizing 2D MBene (Fig. 12b).[126] The authors first synthesized MBene nanosheets by etching out Al from MoAlB followed by ultrasonication. For the first time, they investigated the remarkable DNA adsorption capabilities of MBene for both single-stranded (ssDNA) and double-stranded (dsDNA), and compared these properties with MXenes via Density Functional Theory (DFT) calculations of the adsorption energy (E_{ad}) of four nucleobases of DNA i.e. Adenine (A), Thymine (T), Guanine (G), and Cytosine (C).

Additionally, they designed a paper-based microfluidic point-of-care testing (POCT) device featuring a mixing channel with a constricted-expanded structure, and a lower layer containing a rapid channel (for the dispensation of Exo III, marked yellow) and a slow channel (for the dispensation of MBene, marked blue), ensuring accurate fluid flow. The FAM-DNA probe and ctDNA were introduced into the mixing channel and reacted in the reaction zone, where fluorescence sensing was observed by simply capturing photos with a smartphone and using a custom WeChat application "ctDNA Detection" for RGB value analysis. The authors compared the results of this device with the standard qPCR method using cell and mice serum samples, demonstrating consistency (AUC = 1) and highlighting the device's potential for cancer diagnosis and treatment monitoring. The device showed excellent sensitivity, with a detection range of 0.1 to 100 pm and a limit of detection (LOD) of 0.062 pm.

The Wang group developed a nanozyme-mediated cascading reaction mechanism for ratiometric fluorescence detection of sarcosine, a biological marker for prostate carcinoma (Fig. 12c).[127] MnO_2 nanosheets (NSs) were used to quench the blue fluorescence of carbon dots (BCDs), which served as the core fluorescence detector. The MnO_2 NSs, synthesized by reducing $KMnO_4$ in MOPS solution, exhibited enzyme-like oxidase activity, enabling the conversion of o-phenylenediamine (OPD) to 2,3-diaminophenazine (DAP), producing fluorescence at 562 nm. Sarcosine oxidase (SOD) catalyzed

View Article Online
DOI: 10.1039/D6MA00326E

the oxidative degradation of sarcosine into hydrogen peroxide (H_2O_2), leading to the disintegration of MnO_2 NSs. This resulted in a significant recovery of fluorescence from the BCDs at 440 nm, as the reduced quenching effect of MnO_2 NSs enhanced the fluorescence of DAP at 562 nm. In addition, the fluorescence intensity of BCDs decreased with increasing concentrations of MnO_2 NSs, which likely reduced the fluorescence emission of DAP at 562 nm. The fluorescence-based detector exhibited a linear output in the range of 1 to 80 μM, with a detection limit of 0.36 μM. The approach was further validated using spiked human urine samples, with recovery rates ranging from 94.9% to 98.6%. This study demonstrates a simple, cost effective, and fluorescence sensitive method for detecting H_2O_2-related biological indicators, showing great potential for healthcare diagnostics.

Chen et al. developed a digital droplet microfluidic flow cytometry (Nano-DMFC) device that integrates a 2D metal-organic framework (MOF) nano-sensor for the in-situ detection of microRNAs within circulating tumor cells (CTCs).[130] The device featured a 2D MOF nanosheet that was modified with dual color fluorescent dye labeled DNA biomarkers for fluorescence resonance energy transfer (FRET). A microfluidic droplet generator was used to capture individual breast cancer cells in droplets containing biomodified MOF nanosensors that captured two important tumor markers, miR-21 and miR-10a, through laser induced fluorescence (LIF) detection.

When tested, the sensor was able to detect as few as 10 MCF-7 breast cancer cells amongst 10,000 epithelial cells in a biomimetic serum sample, demonstrating incredible sensitivity. After 23 minutes of processing, the limit of detection (LOD) for miR-21 and miR-10a was 0.54 nM and 0.94 nM respectfully. The nanosensor outperformed for 50 minutes before degrading and had an impressive recovery rate of 86.7 and 92.2 percent for 10 and 30 spiked cells respectively. Importantly, it was able to detect EpCAM negative CTCs, thus lowering the false negatives on detection when compared to EpCAM based flow cytometry.

View Article Online
DOI: 10.1039/D6MA00326E

A novel microfluid based biosensor, comprising of MoS_2 nanosheets grown on MWCNT, is presented by Yang et al. for DNA sensing with high stability and sensitivity (Fig. 12d).[128] The MoS_2/MWCNT nanocomposites were synthesized via a solvent thermal method using N, N-dimethylformamide and $(NH_4)_2MoS_4$, with varying MoS_2/MWCNT ratios (1:20, 1:10, 1:5) tested. The hierarchical structure of the 1:5 MoS_2/MWCNT ratio exhibited the highest quenching ability, enhancing DNA detection capabilities. A microfluidic channel device enabled consistent fluorescence measurements, and the biosensor demonstrated a detection limit of 1 nM and good linearity from 0 to 50 nM. With a sensitivity of detecting DNA as low as 1 fM, this sensor outperformed traditional nanoprobe-based methods in bulk solutions. Additionally, its quenching stability reached 98% after 75 days of storage, significantly surpassing the performance of pure MoS_2 nanosheet solutions. This high-throughput, rapid assay can be completed within minutes, positioning the MoS_2/MWCNT nanocomposite as a promising tool for DNA sensing applications.

4.2 Colorimetric Microfluidic Biosensors

Another emerging optical biosensor gaining attention is the colorimetric or absorbance-based sensor. Colorimetric sensing is widely favoured due to its ease of fabrication, cost-effectiveness, high sensitivity and selectivity, and rapid visual detection. Unlike fluorescence-based methods requiring complex instrumentation and expensive reagents, colorimetric sensors offer easily interpretable output via visible color changes. Their simple operation suits microfluidic platforms for real-time monitoring and efficient biochemical analysis with minimal resources. The high surface area of 2D materials offers abundant active sites, enhancing colorimetric sensitivity.[131] Many 2D materials have demonstrated the ability to mimic peroxidases, exhibiting enhanced enzyme-mimic properties that enable the development of nanozyme-based colorimetric sensors and biosensors.[132,133] Liu et al. developed a microfluidic platform with layered double oxides (LDOs), facilitating colorimetric detection of multiple hepatic biomarkers.[134]

View Article Online
DOI: 10.1039/D5MA00326E

Similarly, Sarah et al. developed a paper-based microfluidic device for the colorimetric detection of alkaline phosphatase (ALP), aspartate aminotransferase (AST), and total serum protein in real blood samples.[135] The vertical flow design enabled a sensitive, affordable, rapid, and equipment-free diagnostic approach. A plastic sheath on the top and bottom layers prevented excess sample intake and evaporation. Lamination sheets with 5.7 mm diameter holes encased a disk filter and patterned paper, properly aligned and sealed. The patterned paper featured three circular hydrophilic zones (~2 mm diameter) surrounded by a hydrophobic wax-based barrier created by heating printed ink to ~150°C for 90 s. The disk filter retained red blood cells, allowing plasma to reach the hydrophilic regions, each containing selective reagents for one biomarker. AST, ALP, and protein assays showed color changes pink, purple, and green respectively only in their designated zones when spiked artificial plasma was used. Real blood samples produced similar colorimetric responses, though measured concentrations were lower than theoretical values.

View Article Online
DOI: 10.1039/D6MA00326E

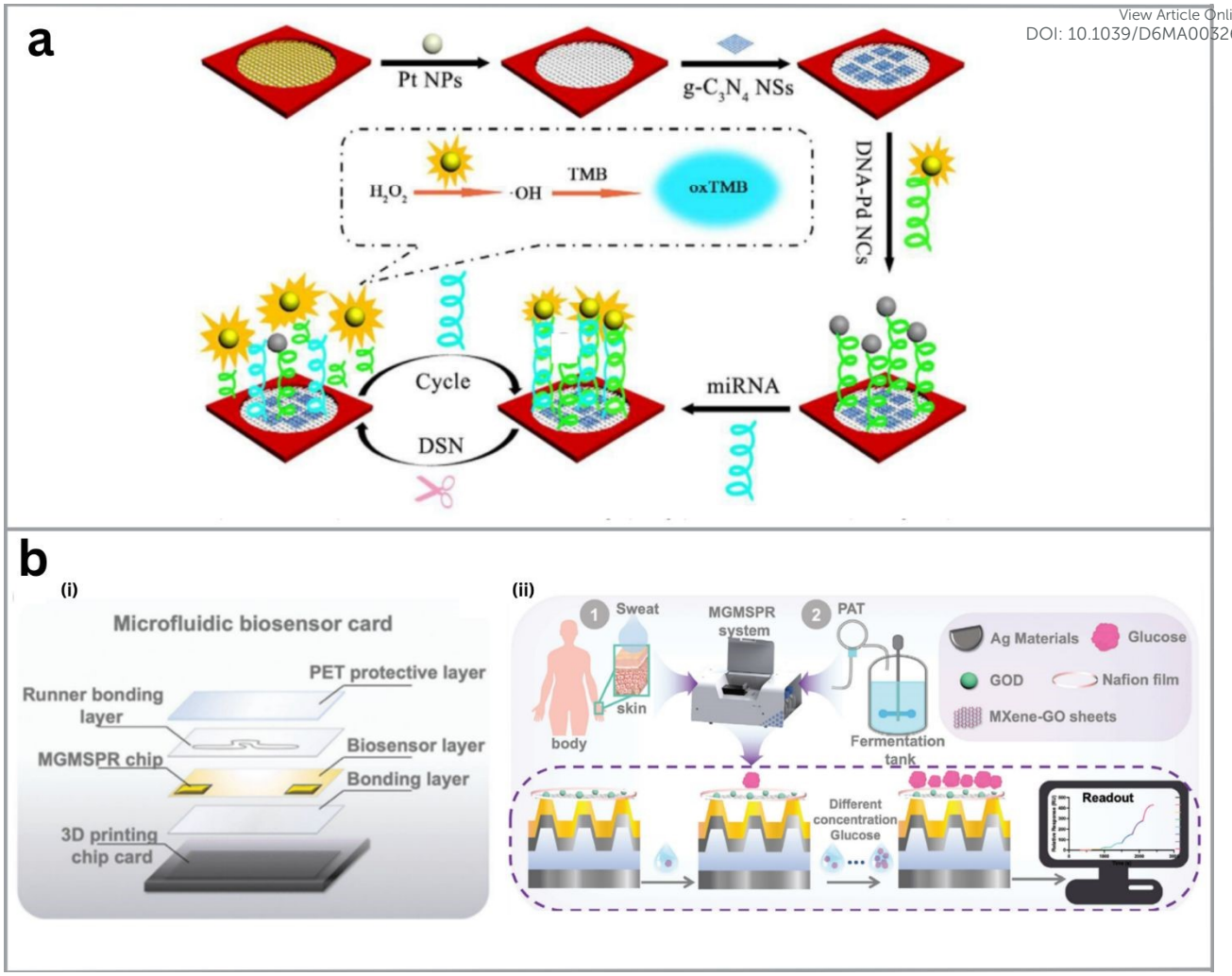

Fig. 13 Optical microfluidic biosensors: (b) PtNPs-modified μPAD for miRNA detection via fluorescence and colorimetric methods.[136] (c) Ti_3C_2 MXene–GO MetaSPR biosensor for sweat glucose monitoring.[137] Adapted from Refs. 136–137 with permission.

MicroRNA (miRNA) plays an important role as a biomarker for the early clinical diagnosis of common diseases like cancer, neurological disorders, and muscle diseases. Recent advances in optical biosensors have enabled dual-mode devices combining absorbance and fluorescence detection. Yin et al. developed a colorimetric and fluorescence dual-mode microfluidic origami paper based analytical device (μPAD) for the quantitative determination of miRNAs (Fig 13a).[136] The μPAD featured distinct reaction, fluorescent, and colorimetric zones. Platinum nanoparticles (Pt NPs) were drop-cast onto the μPAD to suppress background fluorescence. Palladium nanoclusters (Pd NCs), known for their fluorescence and peroxidase-like activity, were immobilized as DNA-Pd NCs. Strong DNA adsorption by g-C_3N_4 led to fluorescence quenching. Upon miRNA introduction, a

View Article Online
DOI: 10.1039/D6MA00326E

DNA-RNA heteroduplex formed and was cleaved via duplex-specific nuclease (DSN)-assisted amplification, releasing DNA-Pd NCs and restoring fluorescence. The freed Pd NSs then catalyzed tetramethylbenzidine (TMB) oxidation with H_2O_2 in the colorimetric zone, producing a visible blue signal. This biosensor exhibited a detection limit as low as 3 fM and strong correlation with logarithmic miRNA concentrations.

Paper-based microfluidic chips, with their pure-color capabilities, offer distinct advantages over conventional microfluidic devices in the development of colorimetric sensors. Haider et al. developed a paper-based biosensor using a dual functional 2D cobalt-terephthalate framework (CoMOF) for glucose detection via colorimetric and fluorometric modes.[138] CoMOF enhanced the catalytic decomposition of H_2O_2 produced by glucose oxidase (GOX) into reactive hydroxyl radicals, which oxidized o-phenylenediamine (OPD) to form a yellow-brown 2,3-diaminophenazine (DAP), indicating glucose presence.

The sensor, prepared by embedding CoMOF and GOX on a 6 mm paper disc, remained stable for 60 days at 4°C, outperforming HRP-based platforms. Upon UV exposure (365 nm), fluorescence was captured via smartphone and analysed with ImageJ, enabling dual-mode quantification with a linear range of 50 µM–15 mM and detection limits of 16.3 µM (colorimetric) and 3.2 (fluorometric). The simple design, minimal sample preparation, and enhanced sensitivity from 2D materials highlight its potential for portable, point-of-care diagnostics.

4.3 Surface Plasmon Resonance (SPR) Based Microfluidic Biosensors

Li et al. developed a novel metasurface plasmon resonance biosensor (MGMSPR) for noninvasive, continuous glucose monitoring (Fig 13b).[137] The biosensor incorporates a dual-channel microfluidic device integrated with heterostructured $Ti_3C_2T_x$-MXene-graphene oxide (MG), enhancing sensitivity to small molecules by optimizing light coupling and amplifying local electric field. To fabricate MGMSPR chips, $Ti_3C_2T_x$-MXene and graphene oxide sheets (1.5 mg/mL) were mixed in varying

View Article Online
DOI: 10.1039/D6MA00326E

weight ratios and applied to the metaSPR surface. The sensing platform featured a dual-channel chip (one test and one reference), with MGMSPR chip affixed to each channel. Flow channels were formed using 100 μm double-sided tape, and PET layer provided structural protection. Glucose detection relied on the enzymatic action of glucose oxidase (GOD), which catalyses glucose to gluconic acid and hydrogen peroxide. As glucose concentration increased, the binding affinity of the GOD cofactor (FAD) decreased, altering the surrounding refractive index. This change was captured through spectral wavelength shifts, enabling real-time glucose monitoring. The sensor achieved a detection limit of 106.8 μM. In contrast, Zhao et al. developed a MoS_2-functionalized TCMF biosensor for T. gondii detection, leveraging refractive index-induced redshifts, distinct from plasmonic SPR, yet comparably sensitive and robust.[139]

Table 3: Optical microfluidic biosensors

Fe^{3+} and AA	MoS_2	Fluorescence Detection		11 μmol/L, 960 nmol/L	20–140 μM, 1–100 μM	[117]
IBV	MoS_2	FRET	Cotton threads	4.6×10^2 EID_{50} / mL	10^2–10^6 EID_{50}/ mL	[118]
Cortisol	MoS_2	FRET	Paper	6.76 ng/mL	10^1–10^3 ng/mL	[119]
DNA	MoS_2	Fluorescence Detection	PDMS	500 pM	0–0.050 μM	[120]
DNA	MoS_2/MWCNTs	Fluorescence Detection	PDMS	1 nM	0–0.050 μM	[124]
AβO	Fe_3O_4/MXene	FRET	PDMS	0.05 nM	0.10–200 nM	[125]
ctDNA	MBene NS	Fluorescence Detection	Paper	0.062pM	1×10^{-1}–1×10^2 pM	[126]
Sarcosine	MnO_2	FRET		0.36 μM	1–80 μM	[127]
DNA	MoS_2/MWCNT	Fluorescence Detection	PDMS	1 nM	0–50 nM	[128]
miR-21 and miR-10a	2D MOF	Fluorescence Detection	PDMS	0.54 nM, 0.94 nM	0–15 nM, 0.2–15 nM	[130]

miRNA	g-C_3N_4	Colorimetry	Paper	3 fM	0.5–1 μM	135
Glucose	MXene-GO	SPR		106.8 μM		137

AA: Ascorbic acid; Fe^{3+}: Iron ions; IBV: Infectious bronchitis virus; AβO: Amyloid β-protein Oligomer; ctDNA: Circulating Tumor DNA; MOF: Metal-Organic Framework; *T. gondii*: *Toxoplasma gondii*.

5. Conclusion and Future Perspective

In this review, we have summarized recent advances in the development of microfluidic biosensors (electrochemical and optical) based on 2D nanostructures beyond graphene such as chalcogenides, MXenes, phosphorene, 2D oxides, and graphene analogs (Table 1 and 2). These materials exhibit exceptional electronic and optical properties, making them promising building blocks for next generation biosensors.

While significant strides have been made, particularly integrating these materials with field-effect transistors (FETs), further efforts are required to translate voltametric, impedance-based, colorimetric and fluorescence sensors into real-world diagnostics applications. These incorporation of 2D materials into microfluidic systems remains technically challenging. Current fabrication methods including drop-casting and surface modification lack precision and scalability, limiting their commercial potential.

Nonetheless, the convergence of 2D materials with soft electronics and flexible substrates opens promising avenues for wearable, non-invasive biosensors capable of continuous monitoring of critical biomarkers. However, key issues such as material stability, signal transduction efficiency, and production cost must be addressed to enable widespread commercialization.

The current landscape predominantly focuses on MoS_2 and MXenes, whereas other 2D materials such as WS_2, $MoSe_2$, and additional transition metal dichalcogenides (TMDs) remain underexplored within microfluidic platforms. Advancing this field requires deeper investigation into these

alternative materials to uncover their unique advantages. Additionally, most 2D material synthesis techniques are limited to laboratory-scale production, underscoring the need for improved, scalable synthesis methods.

Looking ahead, ongoing research into 2D nanomaterials integrated with Lab-on-a-Chip (LOC) platforms holds significant promise for developing highly sensitive, miniaturized, and user-friendly diagnostics for personalized health monitoring and point-of-care (POC) applications.

CRediT Author Contributions

Samrat Sheikh: Writing – original draft, Visualization

Md. Nasiruddin: Conceptualization, Supervision, Writing – original draft, Writing – review & editing

Ibrahim Khan: Writing – original draft

Nusrat Jahan Nipa: Writing – original draft

Fatema Tul Afroz: Writing – original draft

Muhammad Shamim Al Mamun: Conceptualization, Writing – review & editing

Saifullah Mansur: Writing – original draft

Conflicts of interest

The authors declare that there are no conflicts of interest.

Acknowledgements

The authors gratefully acknowledge the Faculty of Science Research Grant, University of Rajshahi, and the Ministry of Science and Technology (MoST), Bangladesh, through the Special Research Grant (Project ID: SRG-253406), for financial support.

View Article Online
DOI: 10.1039/D6MA00326E

References

1 P. Shrimal, G. Jadeja and S. Patel, *Chemical Engineering Research and Design*, 2020, **153**, 728–756.

2 S. Preetam, B. K. Nahak, S. Patra, D. C. Toncu, S. Park, M. Syväjärvi, G. Orive and A. Tiwari, *Biosens. Bioelectron. X*, 2022, **10**, 100106.

3 D. Khorsandi, M. Nodehi, T. Waqar, M. Shabani, B. Kamare, E. N. Zare, S. Ersoy, M. Annabestani, M. F. Çelebi and A. Kafadenk, *J. Nanomater.*, 2021, **2021**, 5537074.

4 S. Haeberle and R. Zengerle, *Lab Chip*, 2007, **7**, 1094–1110.

5 P. S. Dittrich and A. Manz, *Nat. Rev. Drug Discov.*, 2006, **5**, 210–218.

6 F. Dabbagh Moghaddam and F. Romana Bertani, *Materials Chemistry Horizons*, 2022, **1**, 69–88.

7 S. Arshavsky-Graham and E. Segal, in *Microfluidics in Biotechnology*, eds. J. Bahnemann and A. Grünberger, Springer International Publishing, Cham, 2022, pp. 247–265.

8 J. Zhuang, J. Yin, S. Lv, B. Wang and Y. Mu, *Biosens. Bioelectron.*, 2020, **163**, 112291.

9 H. Chen, K. Liu, Z. Li and P. Wang, *Clinica Chimica Acta*, 2019, **493**, 138–147.

10 S. Pagliano, D. E. Marschner, D. Maillard, N. Ehrmann, G. Stemme, S. Braun, L. G. Villanueva and F. Niklaus, *Microsyst. Nanoeng.*, 2022, **8**, 105.

11 M. A. P. Mahmud, S. R. Bazaz, S. Dabiri, A. A. Mehrizi, M. Asadnia, M. E. Warkiani and Z. L. Wang, *Adv. Mater. Technol.*, 2022, **7**, 2101347.

12 S. Nishat, A. T. Jafry, A. W. Martinez and F. R. Awan, *Sens. Actuators B Chem.*, 2021, **336**, 129681.

13 T. Akyazi, L. Basabe-Desmonts and F. Benito-Lopez, *Anal. Chim. Acta*, 2018, **1001**, 1–17.

14 S. Nishat, A. T. Jafry, A. W. Martinez and F. R. Awan, *Sens. Actuators B Chem.*, 2021, **336**, 129681.

15 Anushka, A. Bandopadhyay and P. K. Das, *Eur. Phys. J. Spec. Top.*, 2023, **232**, 781–815.

16 R. Antiochia, *Biosensors (Basel).*, DOI:10.3390/bios11040110.

17 S. Kim and J.-H. Lee, *Biochip J.*, 2022, **16**, 376–396.

18 M. Qing, Y. Yuan, W. Cai, S. Xie, Y. Tang, R. Yuan and J. Zhang, *Sens. Actuators B Chem.*, 2018, **263**, 469–475.

19 E. Heydari-Bafrooei and A. A. Ensafi, *Biosens. Bioelectron. X*, 2023, **13**, 100245.

20 L. Wu, X. Li, H. Miao, J. Xu and G. Pan, *VIEW*, 2022, **3**, 20200170.

21 B. Senf, W.-H. Yeo and J.-H. Kim, *Biosensors (Basel).*, DOI:10.3390/bios10090127.

22 J. Cai, H. Huang, Z. Li, Y. Gao, Q. Liang, X. Chen, N. Chu, W. Hao, D. Wang, Y. Jiang and R. J. Zeng, *Biosens. Bioelectron. X*, 2022, **10**, 100132.

23 M. P. Nair, A. J. T. Teo and K. H. H. Li, *Micromachines (Basel).*, DOI:10.3390/mi13010024.

24 L. Zhang, Y.-C. Zhu and W.-W. Zhao, *Chemosensors*, DOI:10.3390/chemosensors10010014.

25 D. Bhatia, S. Paul, T. Acharjee and S. S. Ramachairy, *Sensors International*, 2024, **5**, 100257.

26 Y. Fu, T. Liu, H. Wang, Z. Wang, L. Hou, J. Jiang and T. Xu, *Journal of Science: Advanced Materials and Devices*, 2024, **9**, 100694.

27 D. Lutomia, R. Poria, D. Kala, P. Garg, R. Nagraik, A. Kaushal, S. Gupta and D. Kumar, *Biosens. Bioelectron. X*, 2025, **24**, 100615.

28 A. Karnwal, R. S. Kumar Sachan, I. Devgon, J. Devgon, G. Pant, M. Panchpuri, A. Ahmad, M. B. Alshammari, K. Hossain and G. Kumar, *ACS Omega*, 2024, **9**, 29966–29982.

29 L. Zheng, G. Cai, S. Wang, M. Liao, Y. Li and J. Lin, *Biosens. Bioelectron.*, 2019, **124–125**, 143–149.

30 H. Aldewachi, T. Chalati, M. N. Woodroofe, N. Bricklebank, B. Sharrack and P. Gardiner, *Nanoscale*, 2018, **10**, 18–33.

31 Y. Lei, T. Zhang, Y.-C. Lin, T. Granzier-Nakajima, G. Bepete, D. A. Kowalczyk, Z. Lin, D. Zhou, T. F. Schranghamer, A. Dodda, A. Sebastian, Y. Chen, Y. Liu, G. Pourtois, T. J. Kempa, B. Schuler, M. T. Edmonds, S. Y. Quek, U. Wurstbauer, S. M. Wu, N. R. Glavin, S. Das, S. P. Dash, J. M. Redwing, J. A. Robinson and M. Terrones, *ACS Nanoscience Au*, 2022, **2**, 450–485.

32 H. Zhang, *ACS Nano*, 2015, **9**, 9451–9469.

33 Y. Lei, T. Zhang, Y.-C. Lin, T. Granzier-Nakajima, G. Bepete, D. A. Kowalczyk, Z. Lin, D. Zhou, T. F. Schranghamer, A. Dodda, A. Sebastian, Y. Chen, Y. Liu, G. Pourtois, T. J. Kempa, B. Schuler, M. T. Edmonds, S. Y. Quek, U. Wurstbauer, S. M. Wu, N. R. Glavin, S. Das, S. P. Dash, J. M. Redwing, J. A. Robinson and M. Terrones, *ACS Nanoscience Au*, 2022, **2**, 450–485.

34 S. Radhakrishnan, M. Mathew and C. S. Rout, *Mater. Adv.*, 2022, **3**, 1874–1904.

35 P. Hess, *Nanoscale Horiz.*, 2021, **6**, 856–892.

36 G. Wang, H. Hou, Y. Yan, R. Jagatramka, A. Shirsalimian, Y. Wang, B. Li, M. Daly and C. Cao, *International Journal of Extreme Manufacturing*, 2023, **5**, 32002.

37 M. Pumera and A. H. Loo, *TrAC Trends in Analytical Chemistry*, 2014, **61**, 49–53.

38 X. Li and H. Zhu, *Journal of Materiomics*, 2015, **1**, 33–44.

39 N. Choudhary, M. A. Islam, J. H. Kim, T.-J. Ko, A. Schropp, L. Hurtado, D. Weitzman, L. Zhai and Y. Jung, *Nano Today*, 2018, **19**, 16–40.

40 W. K. Fan, A. Sherryna and M. Tahir, *ACS Omega*, 2022, **7**, 38158–38192.

41 S. Wang, P. Zeng, X. Zhu, C. Lei, Y. Huang and Z. Nie, *Anal. Chem.*, 2020, **92**, 8819–8826.

42 R. A. Soomro, S. Jawaid, P. Zhang, X. Han, K. R. Hallam, S. Karakuş, A. Kilislioğlu, B. Xu and M. Willander, *Sens. Actuators B Chem.*, 2021, **328**, 129074.

43 S. J. Kim, H.-J. Koh, C. E. Ren, O. Kwon, K. Maleski, S.-Y. Cho, B. Anasori, C.-K. Kim, Y.-K. Choi, J. Kim, Y. Gogotsi and H.-T. Jung, *ACS Nano*, 2018, **12**, 986–993.

View Article Online
DOI: 10.1039/D6MA00326E

1217 44 H. Huang, R. Jiang, Y. Feng, H. Ouyang, N. Zhou, X. Zhang and Y. Wei, *Nanoscale*, 2020, **12**, 1325–
1218 1338.

1219 45 P. Eklund, J. Rosen and P. O. Å. Persson, *J. Phys. D Appl. Phys.*, 2017, **50**, 113001.

1220 46 S. Thurakkal and X. Zhang, *Advanced Science*, 2020, **7**, 1902359.

1221 47 Y. Maruyama, S. Suzuki, K. Kobayashi and S. Tanuma, *Physica B+C*, 1981, **105**, 99–102.

1222 48 J. Kang, J. D. Wood, S. A. Wells, J.-H. Lee, X. Liu, K.-S. Chen and M. C. Hersam, *ACS Nano*, 2015, **9**,
1223 3596–3604.

1224 49 T. Muhmood, I. Ahmad, Z. Haider, S. K. Haider, N. Shahzadi, A. Aftab, S. Ahmed and F. Ahmad,
1225 *Materials Today Sustainability*, 2024, **25**, 100633.

1226 50 N. Muzaffar, A. M. Afzal, H. H. Hegazy and M. W. Iqbal, *J. Energy Storage*, 2023, **64**, 107142.

1227 51 X. Li and H. Zhu, *Journal of Materiomics*, 2015, **1**, 33–44.

1228 52 J. Peng, X. Chen, W.-J. Ong, X. Zhao and N. Li, *Chem*, 2019, **5**, 18–50.

1229 53 A. Jain and A. J. H. McGaughey, *Sci. Rep.*, 2015, **5**, 8501.

1230 54 H. Kiran, A. B. M. Ali, R. Ashraf, M. B. Tahir, M. Nasir, N. Hasnain, M. F. Ullah, D. Abduvalieva and N.
1231 Batool, *J. Inorg. Organomet. Polym. Mater.*, 2025, **35**, 9565–9578.

1232 55 N. Sultana, A. Degg, S. Upadhyaya, T. Nilges and N. Sen Sarma, *Mater. Adv.*, 2022, **3**, 5557–5574.

1233 56 M. Nasiruddin, Z. Wang, H. Waizumi, F. T. Afroz, T. Takaoka, Y. Sainoo, M. Fukuyama and T. Komeda,
1234 *Nanotechnology*, 2024, **35**, 395501.

1235 57 J. Narayan and K. Bezborah, *RSC Adv.*, 2024, **14**, 13413–13444.

1236 58 H. Shen, E. A. López-Guerra, R. Zhu, T. Diba, Q. Zheng, S. D. Solares, J. M. Zara, D. Shuai and Y. Shen,
1237 *ACS Appl. Mater. Interfaces*, 2019, **11**, 373–384.

1238 59 Y. M. Hassan, M. A. Zaghlol and W. M. El-Sayed, *Sens. Biosensing Res.*, 2026, **52**, 101007.

1239 60 A. Chaves, J. G. Azadani, H. Alsalman, D. R. da Costa, R. Frisenda, A. J. Chaves, S. H. Song, Y. D. Kim,
1240 D. He, J. Zhou, A. Castellanos-Gomez, F. M. Peeters, Z. Liu, C. L. Hinkle, S.-H. Oh, P. D. Ye, S. J.
1241 Koester, Y. H. Lee, Ph. Avouris, X. Wang and T. Low, *NPJ 2D Mater. Appl.*, 2020, **4**, 29.

1242 61 C. S. Boland, Y. Sun and D. G. Papageorgiou, *Nano Lett.*, 2024, **24**, 12722–12732.

1243 62 D. Lutomia, R. Poria, D. Kala, P. Garg, R. Nagraik, A. Kaushal, S. Gupta and D. Kumar, *Biosens.*
1244 *Bioelectron. X*, 2025, **24**, 100615.

1245 63 M. Nasiruddin, Z. Wang, H. Waizumi, T. Takaoka, Y. Sainoo, A. Ando, R. Arafune, M. Fukuyama, A.
1246 Hibara and T. Komeda, *ACS Appl. Nano Mater.*, 2023, **6**, 15175–15182.

1247 64 E. M. Hamed and S. F. Y. Li, *ACS Biomater. Sci. Eng.*, DOI:10.1021/acsbiomaterials.4c02465.

1248 65 M. M. Hossain, B. Shabbir, J. Liu, Z. Wan, S. Walia, Q. Bao, T. Alan and S. Mokkapati, *Adv. Mater.*
1249 *Technol.*, 2023, **8**, 2201793.

1250 66 H. Nam, B.-R. Oh, P. Chen, M. Chen, S. Wi, W. Wan, K. Kurabayashi and X. Liang, *Sci. Rep.*, 2015, **5**,
1251 10546.

67 B. Ryu, H. Nam, B.-R. Oh, Y. Song, P. Chen, Y. Park, W. Wan, K. Kurabayashi and X. Liang, *ACS Sens.*, 2017, **2**, 274–281.

68 P. Song, P. Ou, Y. Wang, H. Yuan, S. Duan, L. Chen, H. Fu, J. Song and X. Liu, *Anal. Chim. Acta*, 2023, **1252**, 341036.

69 M. S. Al Mamun, Y. Tanaka, H. Waizumi, T. Takaoka, Z. Wang, M. I. Alam, A. Ando, M. Fukuyama, A. Hibara and T. Komeda, *Phys. Chem. Chem. Phys.*, 2020, **22**, 27724–27731.

70 M. Nasiruddin, H. Waizumi, T. Takaoka, Z. Wang, Y. Sainoo, M. S. Al Mamun, A. Ando, M. Fukuyama, A. Hibara and T. Komeda, *Analyst*, 2023, **148**, 4091–4098.

71 J. Liu, X. Chen, Q. Wang, M. Xiao, D. Zhong, W. Sun, G. Zhang and Z. Zhang, *Nano Lett.*, 2019, **19**, 1437–1444.

72 R. Chand, S. Ramalingam and S. Neethirajan, *Nanoscale*, 2018, **10**, 8217–8225.

73 C. Singh, M. A. Ali, V. Kumar, R. Ahmad and G. Sumana, *Sens. Actuators B Chem.*, 2018, **259**, 1090–1098.

74 H. Jiang, Z. Sun, Q. Guo and X. Weng, *Biosens. Bioelectron.*, 2021, **182**, 113191.

75 S. Ramalingam, A. Elsayed and A. Singh, *Microchimica Acta*, 2020, **187**, 645.

76 H. Chen, B. Luo, S. Wu, S. Shi, Q. Dai, Z. Peng and M. Zhao, *Sensors*, DOI:10.3390/s23115218.

77 T. Hu, M. Zhang, Z. Wang, K. Chen, X. Li and Z. Ni, *Microchemical Journal*, 2020, **158**, 105209.

78 Y. Park, B. Ryu, Q. Deng, B. Pan, Y. Song, Y. Tian, H. B. Alam, Y. Li, X. Liang and K. Kurabayashi, *Small*, 2020, **16**, 1905611.

79 S. Sharma, D. Kar, P. D. Khanikar, A. Moudgil, P. Mishra and S. Das, *ACS Appl. Mater. Interfaces*, 2024, **16**, 30648–30657.

80 R. J. Toh, C. C. Mayorga-Martinez, J. Han, Z. Sofer and M. Pumera, *Anal. Chem.*, 2017, **89**, 4978–4985.

81 J. Liu, X. Jiang, R. Zhang, Y. Zhang, L. Wu, W. Lu, J. Li, Y. Li and H. Zhang, *Adv. Funct. Mater.*, 2019, **29**, 1807326.

82 P. Zhao, J. Zheng, Y. Liang, F. Tian, L. Peng, D. Huo and C. Hou, *ACS Sustain. Chem. Eng.*, 2021, **9**, 15386–15393.

83 Y. Li, Z. Peng, N. J. Holl, Md. R. Hassan, J. M. Pappas, C. Wei, O. H. Izadi, Y. Wang, X. Dong, C. Wang, Y.-W. Huang, D. Kim and C. Wu, *ACS Omega*, 2021, **6**, 6643–6653.

84 M. D. Wagh, R. H, P. S. Kumar, K. Amreen, S. K. Sahoo and S. Goel, *IEEE Sens. J.*, 2022, **22**, 14620–14627.

85 R. Gao, Y. Song, Y. Gao, X. Yang and S.-J. Bao, *Sensors and Actuators Reports*, 2023, **5**, 100146.

86 M. Akhtar, G. Anderson, R. Zhao, A. Alruqi, J. E. Mroczkowska, G. Sumanasekera and J. B. Jasinski, *NPJ 2D Mater. Appl.*, 2017, **1**, 5.

87 V. Sorkin, Y. Cai, Z. Ong, G. Zhang and Y. W. Zhang, *Critical Reviews in Solid State and Materials Sciences*, 2017, **42**, 1–82.

View Article Online
DOI: 10.1039/D6MA00326E

88 S. Ramalingam, R. Chand, C. B. Singh and A. Singh, *Biosens. Bioelectron.*, 2019, **135**, 14–21.

89 X. Zhang, H. Zhi, M. Zhu, F. Wang, H. Meng and L. Feng, *Biosens. Bioelectron.*, 2021, **180**, 113146.

90 X. Wang, W. Deng, L. Shen, M. Yan and J. Yu, *New Journal of Chemistry*, 2016, **40**, 2835–2842.

91 C. Zhou, K. Cui, Y. Liu, L. Li, L. Zhang, S. Hao, S. Ge and J. Yu, *ACS Appl. Mater. Interfaces*, 2021, **13**, 32780–32789.

92 E. Yarali, E. Eksin, H. Torul, A. Ganguly, U. Tamer, P. Papakonstantinou and A. Erdem, *Talanta*, 2022, **241**, 123233.

93 H. Torul, E. Yarali, E. Eksin, A. Ganguly, J. Benson, U. Tamer, P. Papakonstantinou and A. Erdem, *Biosensors (Basel).*, DOI:10.3390/bios11070236.

94 J. S. Nah, S. C. Barman, M. A. Zahed, Md. Sharifuzzaman, H. Yoon, C. Park, S. Yoon, S. Zhang and J. Y. Park, *Sens. Actuators B Chem.*, 2021, **329**, 129206.

95 S. Zhang, M. A. Zahed, Md. Sharifuzzaman, S. Yoon, X. Hui, S. Chandra Barman, S. Sharma, H. S. Yoon, C. Park and J. Y. Park, *Biosens. Bioelectron.*, 2021, **175**, 112844.

96 Q.-F. Li, X. Chen, H. Wang, M. Liu and H.-L. Peng, *ACS Appl. Mater. Interfaces*, 2023, **15**, 13290–13298.

97 Y. Lei, W. Zhao, Y. Zhang, Q. Jiang, J.-H. He, A. J. Baeumner, O. S. Wolfbeis, Z. L. Wang, K. N. Salama and H. N. Alshareef, *Small*, 2019, **15**, 1901190.

98 M. Li, L. Wang, R. Liu, J. Li, Q. Zhang, G. Shi, Y. Li, C. Hou and H. Wang, *Biosens. Bioelectron.*, 2021, **174**, 112828.

99 X. Qiao, Y. Cai, Z. Kong, Z. Xu and X. Luo, *ACS Sens.*, 2023, **8**, 2834–2842.

100 X. Weng, M. Li, L. Chen, B. Peng and H. Jiang, *Talanta*, 2024, **279**, 126675.

101 Z. Ying, L. Qiao, B. Liu, L. Gao and P. Zhang, *Biosens. Bioelectron.*, 2024, **261**, 116502.

102 F. Chen, J. Wang, L. Chen, H. Lin, D. Han, Y. Bao, W. Wang and L. Niu, *Anal. Chem.*, 2024, **96**, 3914–3924.

103 S. Guo, K. Wu, C. Li, H. Wang, Z. Sun, D. Xi, S. Zhang, W. Ding, M. E. Zaghloul, C. Wang, F. A. Castro, D. Yang and Y. Zhao, *Matter*, 2021, **4**, 969–985.

104 Z.-L. Lei and B. Guo, *Advanced Science*, 2022, **9**, 2102924.

105 S. Yu, X. Wu, Y. Wang, X. Guo and L. Tong, *Advanced Materials*, 2017, **29**, 1606128.

106 Q. Ma, G. Ren, K. Xu and J. Z. Ou, *Adv. Opt. Mater.*, 2021, **9**, 2001313.

107 M. Singh, M. Goyal and K. Devlal, *Journal of Taibah University for Science*, 2018, **12**, 470–475.

108 S. Lee, J. Lee, Y. Cao, C. An and S. H. Kang, *Biosens. Bioelectron. X*, 2022, **11**, 100191.

109 O. S. Wolfbeis, *J. Mater. Chem.*, 2005, **15**, 2657–2669.

110 K. E. Sapsford, L. Berti and I. L. Medintz, *Angew. Chem. Int. Ed.*, 2006, **45**, 4562–4589.

111 J. R. Silvius and I. R. and Nabi, *Mol. Membr. Biol.*, 2006, **23**, 5–16.

112 M. Garg, N. Vishwakarma, A. L. Sharma and S. Singh, *ACS Appl. Nano Mater.*, 2021, **4**, 7416–7425.

113 T. Zahra, U. Javeria, H. Jamal, M. M. Baig, F. Akhtar and U. Kamran, *Anal. Chim. Acta*, 2024, **1316**, 342880.

114 M. Garg and N. Pamme, *TrAC Trends in Analytical Chemistry*, 2023, **158**, 116839.

115 H. Deng, X. Yang and Z. Gao, *Analyst*, 2015, **140**, 3210–3215.

116 J. Qiu, P. Jiang, C. Wang, Y. Chu, Y. Zhang, Y. Wang, M. Zhang and L. Han, *Anal. Chem.*, 2022, **94**, 4720–4728.

117 Y. Zhang, S. Zhou, H. Liu, X. Tang, H. Zhou and H. Cai, *Microchemical Journal*, 2021, **169**, 106553.

118 X. Weng and S. Neethirajan, *IEEE Sens. J.*, 2018, **18**, 4358–4363.

119 X. Weng, Z. Fu, C. Zhang, W. Jiang and H. Jiang, *Anal. Chem.*, 2022, **94**, 3526–3534.

120 Y. Huang, Y. Shi, H. Y. Yang and Y. Ai, *Nanoscale*, 2015, **7**, 2245–2249.

121 X. Weng, Y. Kang, Q. Guo, B. Peng and H. Jiang, *Biosens. Bioelectron.*, 2019, **132**, 171–185.

122 S. Catalán-Gómez, M. Briones, S. Cortijo-Campos, T. García-Mendiola, A. de Andrés, S. Garg, P. Kung, E. Lorenzo, J. L. Pau and A. Redondo-Cubero, *Sci. Rep.*, 2020, **10**, 16039.

123 R.-M. Kong, L. Ding, Z. Wang, J. You and F. Qu, *Anal. Bioanal. Chem.*, 2015, **407**, 369–377.

124 D. Yang, M. Tayebi, Y. Huang, H. Y. Yang and Y. Ai, *Sensors*, DOI:10.3390/s16111911.

125 X.-H. Wen, X.-F. Zhao, X.-H. Wang, Y. Wang, J.-C. Guo, H.-G. Zhou, C.-T. Zuo and H.-L. Lu, *ACS Appl. Nano Mater.*, 2022, **5**, 15925–15933.

126 S. Yang, J. Zhu, L. Zhao, L. Yang, H. Fa, Y. Wang, D. Huo, C. Hou, D. Zhong and M. Yang, *Adv. Funct. Mater.*, 2025, **35**, 2415074.

127 W. Li, T. Li, S. Chen, D. Deng, Y. Ji and R. Li, *Sens. Actuators B Chem.*, 2022, **355**, 131341.

128 D. Yang, M. Tayebi, Y. Huang, H. Y. Yang and Y. Ai, *Sensors*, DOI:10.3390/s16111911.

129 M. S. Javed, X. Zhang, T. Ahmad, M. Usman, S. S. A. Shah, A. Ahmad, I. Hussain, S. Majeed, M. R. Khawar, D. Choi, C. Xia, W. Al Zoubi, M. A. Assiri, A. M. Hassan, S. Ali and W. Han, *Materials Today*, 2024, **74**, 121–148.

130 J. Chen, G. Oudeng, H. Feng, S. Liu, H.-W. Li, Y.-P. Ho, Y. Chen, Y. Tan and M. Yang, *Small*, 2022, **18**, 2201779.

131 D. Zhu, B. Liu and G. Wei, *Biosensors (Basel).*, DOI:10.3390/bios11080259.

132 W. Zhang, X. Li, T. Cui, S. Li, Y. Qian, Y. Yue, W. Zhong, B. Xu and W. Yue, *Microchimica Acta*, 2021, **188**, 174.

133 S. Li, Z. Chen, F. Yang and W. Yue, *Microchemical Journal*, 2023, **194**, 109247.

134 X. Liu, X. Mei, J. Yang and Y. Li, *ACS Appl. Mater. Interfaces*, 2022, **14**, 6985–6993.

135 S. J. Vella, P. Beattie, R. Cademartiri, A. Laromaine, A. W. Martinez, S. T. Phillips, K. A. Mirica and G. M. Whitesides, *Anal. Chem.*, 2012, **84**, 2883–2891.

136 X. Yin, L. Liang, P. Zhao, F. Lan, L. Zhang, S. Ge and J. Yu, *J. Mater. Chem. B*, 2018, **6**, 5795–5801.

137 R. Li, H. Fan, Y. Chen, S. Yin, G. L. Liu, Y. Li and L. Huang, *Advanced Science*, 2025, **12**, 2410376.

138 H. A. J. Al Lawati and J. Hassanzadeh, *Anal. Chim. Acta*, 2020, **1139**, 15–26.

139 H. Chen, B. Luo, S. Wu, S. Shi, Q. Dai, Z. Peng and M. Zhao, *Sensors*, DOI:10.3390/s23115218.

View Article Online
DOI: 10.1039/D6MA00326E

Data Availability Statement

Data sharing is not applicable to this article as no new data were created or analyzed in this study.